

NASA TECHNICAL NOTE

NASA TN D-6462



NASA TN D-6462

C.1



LOAN COPY: RET  
AFWL (DO  
KIRTLAND AFB, N. M.

EXPERIMENTAL LAMINAR, TRANSITIONAL,  
AND TURBULENT BOUNDARY-LAYER PROFILES  
ON A WEDGE AT LOCAL MACH NUMBER 6.5  
AND COMPARISONS WITH THEORY

*by Michael C. Fischer and Dal V. Maddalon*

*Langley Research Center*

*Hampton, Va. 23365*



0133296

1. Report No. NASA TN D-6462		2. Government Accession No.		3. Recipient's Catalog No.	
4. Title and Subtitle EXPERIMENTAL LAMINAR, TRANSITIONAL, AND TURBULENT BOUNDARY-LAYER PROFILES ON A WEDGE AT LOCAL MACH NUMBER 6.5 AND COMPARISONS WITH THEORY				5. Report Date September 1971	
				6. Performing Organization Code	
7. Author(s) Michael C. Fischer and Dal V. Maddalon				8. Performing Organization Report No. L-7776	
9. Performing Organization Name and Address NASA Langley Research Center Hampton, Va. 23365				10. Work Unit No. 136-13-01-11	
				11. Contract or Grant No.	
12. Sponsoring Agency Name and Address National Aeronautics and Space Administration Washington, D.C. 20546				13. Type of Report and Period Covered Technical Note	
				14. Sponsoring Agency Code	
15. Supplementary Notes					
16. Abstract Boundary-layer pitot surveys were obtained at numerous stations along a wedge at $10^\circ$ total incidence in helium at nominal free-stream and local Mach numbers of 20 and 6.5, respectively. Local unit Reynolds number per centimeter varied from $0.056 \times 10^6$ to $0.255 \times 10^6$ and wall temperatures were nearly adiabatic. Mach number, density, and velocity profiles indicate that the boundary layer varied along the surface from laminar to fully turbulent for all but the lowest of four unit Reynolds number test cases. Experimental Mach number, density, and velocity profile shapes and integral thickness parameters along the wedge at two unit Reynolds number test cases were compared with predictions of a finite-difference computation method. These comparisons indicated the need for improved eddy viscosity models to represent better the high-intensity turbulent fluctuations which apparently occur in the transition region. Theoretical predictions of laminar displacement and momentum thicknesses were approximately 30 percent and 35 percent, respectively, below experimental results. This discrepancy may be due to the influence of the finite leading-edge thickness on boundary-layer development.					
17. Key Words (Suggested by Author(s)) Boundary-layer profiles Boundary-layer transition Theoretical predictions Adiabatic wall			18. Distribution Statement Unclassified - Unlimited		
19. Security Classif. (of this report) Unclassified		20. Security Classif. (of this page) Unclassified		21. No. of Pages 58	22. Price* \$3.00

EXPERIMENTAL LAMINAR, TRANSITIONAL, AND  
TURBULENT BOUNDARY-LAYER PROFILES ON A WEDGE AT LOCAL  
MACH NUMBER 6.5 AND COMPARISONS WITH THEORY

By Michael C. Fischer and Dal V. Maddalon  
Langley Research Center

SUMMARY

In order to provide test cases for computation methods and to examine the structure of laminar, transitional, and turbulent hypersonic boundary layers, pitot surveys were obtained on a wedge placed at  $10^\circ$  total incidence in helium flow at a nominal free-stream Mach number of 20. The tests were conducted over a range of local unit Reynolds number per centimeter of  $0.056 \times 10^6$  to  $0.255 \times 10^6$  at near-adiabatic wall conditions with the total temperature varying slightly from  $345^\circ$  K to  $354^\circ$  K and with a ratio of wall temperature to total temperature of about 0.85. The local Mach number varied from 6.2 to 6.7.

Mach number, density, and velocity profiles computed from the pitot surveys and the assumption of a Crocco relation between total temperature and velocity indicate that the boundary layer varied from laminar to fully turbulent along the wedge surface for all but the lowest of four unit Reynolds number test cases ( $Re/cm = 0.056 \times 10^6$  to  $0.255 \times 10^6$ ). For the lowest unit Reynolds number case, the boundary layer was still in a transitional state near the rear of the wedge. Experimental Mach number, density, and velocity profile shapes along the wedge at the lowest and highest unit Reynolds number test cases showed fair agreement with profiles predicted by a finite-difference computation method. Agreement of predicted and experimental boundary-layer-thickness parameters was not so good. These comparisons show that a need exists for improved eddy viscosity models through the transition region to represent better the high-intensity turbulent fluctuations which apparently exist in this region at hypersonic Mach numbers. Theoretical predictions of laminar displacement and momentum thickness were approximately 30 percent and 35 percent, respectively, below experimental results. The downstream effect of a finite leading-edge thickness on boundary-layer-profile shape and growth may have caused this discrepancy.

INTRODUCTION

The development of a boundary layer from laminar to turbulent flow has received considerable attention both experimentally and theoretically in the past. In recent years,

nonsimilar computation methods have been developed which can compute the downstream development of transitional and turbulent compressible boundary-layer flows with initial laminar profiles and pertinent free-stream and local conditions as inputs (refs. 1 and 2). In order to model the turbulence terms in the transition region, the eddy viscosity function is biased with a streamwise intermittency factor which varies from 0 to 1.0 through the transition region. To test and to improve the accuracy of these and other computation methods (refs. 3 to 5) require accurate experimental test cases. However, only a limited number of test cases have been obtained on axisymmetric or two-dimensional bodies at hypersonic Mach numbers ( $M_e > 5$ ) and these test cases typically include only a few surveys in the transitional and turbulent regime. (See refs. 6 to 16.)

This need gave impetus to initiation of the present investigation to provide detailed test cases for the development of computation methods and the examination of the structure of a hypersonic boundary layer developing from a laminar to a turbulent state. Boundary-layer pitot surveys were obtained at numerous stations on a  $5^\circ$  half-angle wedge with the test surface placed at  $10^\circ$  incidence to a nominal Mach 20 helium free-stream flow. Local unit Reynolds number per centimeter varied from  $0.056 \times 10^6$  to  $0.255 \times 10^6$  for a range of stagnation chamber pressure from 3.55 to 20.79 MN/m<sup>2</sup>. Stagnation temperature was essentially constant, varying only between  $345^\circ$  K and  $354^\circ$  K.

#### SYMBOLS

$C_f$	skin-friction coefficient
$d$	diameter of circular pitot probe
$h$	height of oval pitot probe
$M$	Mach number
$N_{Pr}$	Prandtl number
$p$	pressure
$R$	Reynolds number
$Re_{,\theta}$	Reynolds number based on momentum thickness
$T$	temperature

$u$	local velocity in the $x$ -direction
$x$	distance along wedge surface from leading edge
$y$	perpendicular distance from wedge surface
$\Gamma$	intermittency function (used in computation method of ref. 1)
$\delta$	boundary-layer thickness determined from pitot profile, $dp_{t,2}/dy = 0$
$\delta^*$	boundary-layer displacement thickness
$\epsilon$	angle between shock wave and free stream
$\theta$	boundary-layer momentum thickness
$\mu$	viscosity
$\rho$	density

Subscripts:

2	behind normal shock
E,tr	end of transition
e	conditions at boundary-layer edge
i	initial conditions at $x = 0$
l	local conditions within boundary layer
t	stagnation conditions
S,tr	start of transition
w	wall
$\infty$	free stream, ahead of shock

## TEST FACILITY

The experimental investigation was conducted in the Langley 22-inch helium tunnel which has an axisymmetric contoured nozzle and a nominal test-section Mach number of 20. The diameter of the test section is 55.9 cm and the free-stream Mach number varies with stagnation pressure from about 16.1 at  $0.517 \text{ MN/m}^2$  to 21.7 at  $20.79 \text{ MN/m}^2$ . For this pressure range in unheated flow, the free-stream Reynolds number per centimeter varies from  $0.020 \times 10^6$  to  $0.556 \times 10^6$ . Free-stream stagnation temperature can be varied over the range of  $300^\circ \text{ K}$  to  $450^\circ \text{ K}$ . A detailed description and calibration of the facility is presented in reference 17.

## MODELS

Two separate models were used in this investigation: a pressure model and a boundary-layer survey model. Both models were fabricated from inconel with a 0.0051-cm leading-edge thickness; the skin thicknesses of the pressure and survey models were 0.160 cm and 0.076 cm, respectively. The pressure model was a smooth  $5^\circ$  half-angle wedge with a width of 27.94 cm and a length of 40.64 cm and was instrumented with 12 pressure orifices along the model center line. The orifice tubing of 0.152 cm outside diameter (o.d.) and 0.102 cm inside diameter (i.d.) was stepped up to tubing of 0.317 cm o.d. and 0.229 cm i.d. a short distance from the surface. A detailed measurement of the surface of the pressure model revealed a local depression in the center-line region beginning at about  $x = 30.5 \text{ cm}$  and ending at about  $x = 38.1 \text{ cm}$ . The maximum depth of this depression was about 0.038 cm. The effect of this depression on the pressure measurements is discussed in a later section. The initial boundary-layer survey model was identical in external geometry to the pressure model and was instrumented with thermocouples along the center line. Heat-transfer studies indicated that the boundary layer did not become fully turbulent on the 40.64-cm-long wedge model; therefore, a 20.32-cm-long extension was added for a total length of 60.96 cm. Boundary-layer surveys were obtained at three stations on the 40.64-cm-long wedge, and surveys were also obtained at four stations on the rearward half of the 60.96-cm wedge configuration. Measurements of the surfaces of the 40.64-cm and 60.96-cm wedge survey models indicated excellent surface uniformity. In an effort to maintain uniform two-dimensional flow on the model surface, swept end plates were used and the wedge models were side mounted to the tunnel wall. A sketch of the 60.96-cm survey model mounted in the tunnel is shown in figure 1(a), and the locations of the survey and pressure measuring stations are presented in figure 1(b).

## TEST CONDITIONS, PROCEDURE, AND INSTRUMENTATION

Pitot pressure surveys through the boundary layer were obtained in a heated free-stream flow with near-adiabatic model wall conditions,  $T_w/T_{t,\infty} \approx 0.85$ . A total of seven stations were surveyed along the 40.64-cm- and 60.96-cm-long wedge surfaces from  $x = 9.91$  cm to  $x = 59.94$  cm. Surveys at  $x = 9.91$  cm, 18.03 cm, and 22.86 cm were obtained on the 40.64-cm wedge while surveys at  $x = 43.18$  cm, 48.26 cm, 53.34 cm, and 59.94 cm were obtained on the 60.96-cm wedge configuration. Local unit Reynolds number per centimeter varied from  $0.056 \times 10^6$  to  $0.255 \times 10^6$  for a range of stagnation pressure from 3.55 to 20.79 MN/m<sup>2</sup>. Free-stream Mach number on the tunnel center line varied from 19.1 to 21.7, depending on the unit Reynolds number. Stagnation temperature was essentially constant with values between 345° K and 354° K. Details of the test conditions are given in table 1.

Boundary-layer pitot surveys were conducted with two different size probes. For the 40.64-cm-long wedge, a 0.102-cm-o.d., 0.051-cm-i.d. probe was used to survey the boundary layer at three stations:  $x = 9.91$  cm, 18.03 cm, and 22.86 cm. For the 60.96-cm-long wedge configuration (20.32-cm-long extension added to 40.64-cm-long wedge), a 0.229-cm-o.d., 0.178-cm-i.d. probe was used to survey the boundary layer at four stations:  $x = 43.18$  cm, 48.26 cm, 53.34 cm, and 59.94 cm. Details of the survey apparatus are given in figure 2. Once the pressures settled out at any given station and a reading was obtained, the probe was traversed to a new position at that station. Typical run time was about 30 sec. During this test run time, the model wall temperature varied a maximum of about 4° K. Additional runs were made to obtain wall static pressure on the 40.64-cm-long wedge pressure model. Pressure transducers with a capacitive sensing circuit were used to measure pressures less than about 6000 N/m<sup>2</sup>, with an accuracy of about  $\pm 1.0$  percent of full scale; whereas all pressures greater than about 6000 N/m<sup>2</sup> were measured with strain-gage diaphragm-type pressure transducers, with an accuracy of  $\pm 0.25$  percent of full scale. Tunnel total pressure was measured in the settling chamber with both strain-gage diaphragm-type pressure transducers and a Bourdon gage. Free-stream total temperature was measured in the test section with a 0.317-cm-o.d. shielded iron-constantan total-temperature probe. Corrections to the temperatures measured with this probe were insignificant since the recovery factor was approximately 1.

## DATA REDUCTION PROCEDURE

### Corrections to Pitot Data

The measured pitot data were analyzed for possible real gas, viscous interaction, and rarefaction effects. Viscous interaction and rarefaction effects may be significant

in low-density regions within the boundary layer, as shown in reference 18. The magnitude of the viscous and rarefaction effects depends primarily on the local Mach number and local Reynolds number based on probe diameter. For this investigation, the smallest local Reynolds number in the boundary layer based on probe diameter was  $R_{\ell,d} = 44$  which occurs at  $M_{\ell} = 0.74$ . If the viscous interaction and rarefaction correction curves presented by Beckwith, Harvey, and Clark (ref. 19) for nitrogen and air test gases are assumed to be roughly applicable to the present helium case, the corrections to the pitot data near the model wall of the present study were less than 2 percent and are therefore neglected. Probe interference effects are discussed in a later section of this report.

Real-gas effects are a function of the total-pressure and total-temperature level. Local total pressures at the boundary-layer edge are small because of the strong wedge shock. The real-gas corrections to the pitot data near the boundary-layer edge were therefore less than 1 percent (ref. 20) and are considered negligible.

### Static Pressure

The measured values of wall static pressure are presented in figure 3. As previously mentioned, the wedge pressure model was only 40.64 cm long. From the pressure distributions in figure 3, it is evident that the surface depression near the rear of the pressure model, discussed in a previous section, causes the pressure expansion and subsequent compression measured near the rear of this model.

Measured surface pressures were considerably higher than inviscid predicted values (fig. 3). The laminar viscous interaction predictions of Bertram (ref. 21) are generally in good agreement with the measured pressures at the two highest unit Reynolds numbers. Pitot pressure profile data obtained at each of the four unit Reynolds numbers were reduced to Mach number profiles with constant static pressure across the boundary layer being assumed. Static pressures used for this purpose were obtained from faired curves (shown in fig. 3) through the measured pressure data ignoring the last three measured wall pressures, which were apparently affected by the surface depression. These fairings were extended to  $x = 59.94$  cm, which was the last boundary-layer survey station.

### Boundary-Layer Profile Parameters

As stated, Mach number profiles were calculated from the measured pitot data by using the static pressures obtained from fairings through the measured wall static pressures. Velocity and density profiles were computed from the calculated Mach number profiles by assuming a Crocco total-temperature—velocity distribution

$$\frac{T_{t,\ell} - T_w}{T_{t,\infty} - T_w} = \frac{u_{\ell}}{u_{\infty}}$$

since this type of distribution is typical of zero-pressure-gradient flows with constant wall temperature (refs. 3 and 22). The edge of the boundary layer was taken as the location where  $dp_{t,2}/dy = 0$ . A summary of the free-stream and local test conditions and the computed boundary-layer parameters  $\delta^*$  and  $\theta$  are given in table 1. Free-stream unit Reynolds numbers were calculated from the measured stagnation conditions and the viscosity corrected for quantum effects (ref. 23). Local unit Reynolds numbers at the boundary-layer edge were calculated by using the measured pitot pressure at the edge of the boundary layer and the faired wall static pressure. For each of the four unit Reynolds number test cases, the local pitot pressure at the boundary-layer edge varied slightly with  $x$  as did the wall pressure so that the local computed values of Mach number and Reynolds number also varied slightly. Average values of local Mach number and Reynolds number are presented in table 1 for simplicity. However, table 2 presents the profile data at every station for each of the four unit Reynolds numbers and also lists the actual local Mach number and Reynolds number for each survey station. The boundary-layer displacement thickness and momentum thickness were calculated from the expressions

$$\delta^* = \int_0^{\delta} \left( 1 - \frac{\rho u}{\rho_e u_e} \right) dy$$

$$\theta = \int_0^{\delta} \frac{\rho u}{\rho_e u_e} \left( 1 - \frac{u}{u_e} \right) dy$$

## RESULTS AND DISCUSSION

Mach number, density, and velocity profiles calculated from the pitot surveys obtained at  $Re/cm = 0.056 \times 10^6$  are shown in figure 4. Also shown are theoretical laminar profiles obtained by the method of reference 1. All experimental data have been normalized by the experimentally determined displacement thicknesses, whereas the theoretical solution results were normalized by the theoretical displacement thicknesses.

In figure 4(c) a 1/15-power-law velocity profile is shown which is typical of velocity profiles at the end of transition for the local Reynolds number, Mach number, and wall temperature ratio of this investigation. (See ref. 24.) The N-power-law velocity profile typically peaks in value at the end of transition and then decreases downstream of this location as the boundary layer relaxes (ref. 24). The boundary layer apparently was laminar at the first three stations for this lowest unit Reynolds number case (fig. 4), with transition occurring after 22.86 cm. The start-of-transition location determined from heat-transfer data for this unit Reynolds number (reported in ref. 25) is 25.40 cm, which agrees with the location indicated by the profile data. The velocity profiles measured at the most rearward stations are in reasonable agreement with the 1/15-power-law turbulent

profile in the outer part of the boundary layer. Hence, the outer part of the boundary layer at these stations is apparently near fully turbulent conditions.

For the next unit Reynolds number test case,  $Re/cm = 0.101 \times 10^6$ , shown in figure 5, comparison of the profiles indicates that the boundary layer was laminar at the first station, and the beginning of transitional flow occurred near  $x = 18.03$  cm. This result is in agreement with the heat-transfer data of reference 25 which further indicate that the end of transition occurred at  $x = 51.60$  cm. Once again the velocity profile data at the rearward stations show reasonable agreement with the 1/15-power-law turbulent profile.

Boundary-layer profiles obtained at the highest unit Reynolds numbers,  $Re/cm = 0.149 \times 10^6$  and  $Re/cm = 0.255 \times 10^6$ , are shown in figures 6 and 7. The profiles at both unit Reynolds numbers indicate a laminar boundary layer at only the first survey station,  $x = 9.91$  cm, and a fully turbulent boundary layer over the last half of the wedge surface. As with the previous test cases, the approximate location of the start and end of transition determined from the profiles agreed with the transition locations deduced from the heat-transfer data of reference 25. In addition, the 1/15-power-law turbulent velocity profiles again display reasonable agreement in the outer part of the boundary layer with the computed velocity profiles (figs. 6(c) and 7(c)). Note, however, that the velocity profiles measured at the last three survey stations at  $Re/cm = 0.255 \times 10^6$  are less full than those measured at the last three survey stations at  $Re/cm = 0.149 \times 10^6$ . In both cases, the three surveys were obtained in a fully turbulent boundary layer, but for the  $Re/cm = 0.255 \times 10^6$  case the last three velocity profiles are farther downstream of the end of transition location so that the turbulent boundary layer has relaxed somewhat (higher  $Re_{\theta}$ ) with a subsequent reduction in the N-power-law profile. (See ref. 24.)

The distribution of the experimentally determined displacement and momentum thickness along the wedge surface for each of the four-unit Reynolds number test cases is presented in figure 8. Displacement and momentum thickness obtained from the data on the 60.96-cm wedge configuration show a continuation of the trend obtained from the data measured on the 40.64-cm wedge configuration.

#### Assessment of Probe Interference Effects

Numerous factors could be adversely influencing the measured pitot pressures. The effects of viscous interaction and rarefaction (low Reynolds and Mach number effects) as well as real-gas effects were analyzed for the present test conditions in a previous section of this paper and found to be negligible. With a probe placed in a boundary layer, there will be some disturbance to the flow and a resulting error in pitot pressure regardless of how small the probe. Such effects are generally largest near the wall (possible

boundary-layer separation) and are evident in the laminar velocity profile data closest to the wall (solid symbols in figs. 4(c), 5(c), and 6(c)). As a check on the determination of the boundary-layer thicknesses, the laminar boundary-layer velocity profiles at the lowest unit Reynolds number (fig. 4(c)) were recomputed by neglecting the pitot data near the wall (solid symbols in fig. 4(c)) and fairing the pitot profile into the measured wall static pressure value. The resulting effect on  $\delta^*$  and  $\theta$  was negligible.

If the pitot probe diameter is large compared with the boundary-layer thickness, distorted boundary-layer profiles will result and an overshoot or peak in pitot pressure occurs at the boundary-layer edge (refs. 26 to 28). The distortion in the measured profile may cause  $\theta$  and  $\delta^*$  to be greater than the true value (refs. 26 to 28) and the overshoot or peak in pitot pressure at the boundary-layer edge may be accompanied by an apparent increase in  $\delta$  (ref. 26). The magnitude of the increase in  $\delta^*$  and  $\theta$  from the true value depends primarily on the ratio of the probe height  $h$  or diameter  $d$  to the boundary-layer thickness  $\delta$ . Results of reference 29 indicate that, with an oval probe of height  $h$  and width  $5h$ , the ratio of probe height to boundary-layer thickness  $h/\delta$  could be as large as 0.22 without adversely affecting the pitot pressure reading in the laminar boundary layer on a hollow cylinder at  $M_\infty = 2.41$ . Blue and Low (ref. 28) showed that on a flat plate at  $M_\infty = 3$  accurate surveys could be obtained with an oval probe of height  $h$  and width  $5h$  with  $h/\delta$  up to 0.26. Monaghan (ref. 26) analyzed the data of Blue and Low and formulated a correction for  $\theta$  and  $\delta^*$  of the form

$$\frac{\theta_{\text{meas}}}{\theta_{\text{true}}} \quad \text{or} \quad \frac{\delta^*_{\text{meas}}}{\delta^*_{\text{true}}} = \left(1 - \frac{h}{\delta}\right)^{-0.18}$$

Substituting the values of  $d/\delta$  for the present investigation indicates that the measured values of  $\delta^*$  and  $\theta$  could be from 3 percent to 8 percent greater than the true values due to probe size effects. One questions the applicability of this correction factor to the present hypersonic results since the formulation was based on supersonic results with oval-shaped probes; therefore, no corrections of this type were made to the integral parameters  $\delta^*$  and  $\theta$ . However, the boundary-layer surveys of the present investigation did exhibit overshoots or peaks in pitot pressure at the boundary-layer edge when  $d/\delta \geq 0.19$ ; thus, the presence of either probe effects or a nonuniform inviscid flow due to viscous-inviscid interaction is indicated. Based on the study of reference 26, the pitot pressure profiles of this investigation were faired at the boundary-layer edge to eliminate these peaks as shown in figure 9. For the lowest unit Reynolds number test case, only the pitot profile at the first survey station was faired at the boundary-layer edge. Pitot profiles at both the first and second survey stations were faired for the three remaining unit Reynolds number test cases.

## Comparison of Experimental Profiles With Results of Numerical Solutions

The pitot profiles measured along the wedge surface provide test cases for nonsimilar finite-difference computation methods which predict the development of a boundary layer through the laminar, transitional, and turbulent regions given initial laminar profiles and downstream boundary conditions. The finite-difference computation method of Harris (ref. 1) was used to compute profiles for the lowest and highest unit Reynolds number cases. This method uses a two-layer eddy viscosity model. In the inner region of the boundary layer, the conventional Prandtl mixing length slope of 0.4 is used in conjunction with the van Driest damping function evaluated at wall conditions; the eddy viscosity in the outer layer is based on the Clauser model. An intermittency function  $\Gamma$  biases the eddy viscosity through the transition region. Inputs required for this computation method are given in table 3 and include the measured wall pressure distribution, the initial edge Mach number (computed from pitot pressure data), and transition locations determined from heat-transfer data of reference 25. A subroutine of the program calculates similar laminar profiles which are then used as initial profiles at the origin.

The numerical method underpredicted  $\delta$ ,  $\delta^*$ , and  $\theta$  in the laminar region. In order to match the predicted  $\delta^*$  and the experimental  $\delta^*$  at the last laminar profile station, laminar numerical solutions were obtained over the entire length of the wedge for both unit Reynolds number cases. An x-coordinate system was then established for the numerical method so that the predicted  $\delta^*$  and the experimental  $\delta^*$  at the last laminar survey station were equal. The resulting increases in the lengths of laminar flow for the numerical method were 10.6 cm and 11.6 cm for the low and high Reynolds number cases, respectively. The pressure distributions in figure 3 were not shifted to match the new coordinate system since the pressure gradients are small in the regions where the profiles are compared.

In the reduction of the experimental profiles, a Crocco total-temperature—velocity relationship, which implies  $N_{Pr,t} = 1.0$ , was assumed, whereas the predicted results (ref. 1) were computed both with a Rotta turbulent Prandtl number distribution (ref. 30),  $N_{Pr,t} = 0.95 [1 - 0.5(y/\delta)^2]$ , and with  $N_{Pr,t} = 1.0$  to provide some indication of the effect of turbulent Prandtl number on profile shape.

The experimentally determined Mach number, density, and velocity profiles at  $R_e/cm = 0.056 \times 10^6$  are compared with the predicted results of the computation method in figure 10. The experimental  $\delta^*$  is used to normalize both experimental and predicted results so that the comparisons are made on a y-dimensional basis. The first profile shown is laminar, where the theoretical and experimental values of  $\delta^*$  were matched. Transition was initiated at  $x = 25.4$  cm (fig. 4(c)) which corresponds to  $x = 36.0$  cm in the calculation. Since there was no established end of transition location for this low unit Reynolds number case, it was assumed in the computation method that

$x_{E,tr}/x_{S,tr} = 1.35$ . This ratio is lower than normally encountered but is not completely unreasonable and was used because it resulted in good comparison of predicted and experimental  $\delta^*$  along the wedge. The prediction with the variable  $N_{Pr,t}$  is shown for all the experimental stations. For comparison, two additional predictions are presented at the last survey station; the first with the same transition zone length but with  $N_{Pr,t} = 1.0$ , whereas the second case has  $N_{Pr,t} = 1.0$  but a longer transition zone length with  $x_{E,tr}/x_{S,tr} = 2.4$ . In general, the predicted profiles are in fair agreement with the measured profiles. The Mach number and density profiles are not predicted too well in the inner and outer portions of the boundary layer (figs. 10(a) and 10(b)) with too low a predicted boundary-layer thickness at the downstream stations. The predicted velocity profiles are either somewhat too full or not full enough in the lower half of the boundary layer (fig. 10(c)). Predicted results at the last survey station with  $x_{E,tr}/x_{S,tr} = 1.35$  and  $N_{Pr,t} = 1.0$  and with  $x_{E,tr}/x_{S,tr} = 2.4$  and  $N_{Pr,t} = 1.0$  indicate that increasing the transition zone decreases the agreement between prediction and experiment because of the reduced growth of  $\delta^*$  and  $\delta$  along the surface. The use of  $N_{Pr,t} = 1.0$  instead of Rotta's  $N_{Pr,t}$  distribution contributes only slightly to the increased disagreement and had a negligible effect on the velocity profiles.

The highest unit Reynolds number test case (fig. 11) shows worse agreement with the predicted Mach number, density, and velocity profiles than the low unit Reynolds number case. The predicted growth of  $\delta^*$  and  $\delta$  along the wedge is somewhat different from the experimental results, especially in the transition region, so that on a dimensional basis the predicted profiles exhibit considerable disagreement. (See figs. 11(a) to 11(c).) The length of the transition zone, or the ratio  $x_{E,tr}/x_{S,tr} = 2.85$ , used as an input to the prediction method was obtained from heat-transfer data (ref. 25).

Also shown at the last survey station are results from the computation method with  $x_{E,tr}/x_{S,tr} = 2.85$  and  $N_{Pr,t} = 1.0$  which indicate that the choice of turbulent Prandtl number had little effect on the Mach number and density profiles and negligible effect on the velocity profiles. The predicted values of  $\delta^*$  and  $\theta$  are compared with the experimental results for both unit Reynolds number test cases in figure 12. In each case, the predicted  $\delta^*$  was matched with the experimental  $\delta^*$  at the first station. The disagreement between experiment and prediction is clearly evident as well as the weak effect of turbulent Prandtl number on boundary-layer development. A possible cause for the disagreement between the predicted and experimental profile shapes and integral parameter thicknesses along the wedge may be the finite leading-edge thickness and the subsequent curved shock—boundary-layer interaction. These effects are discussed in a later section of this report.

The results of the comparisons of experimental and predicted profiles in figures 10 and 11 suggest that the computation method needs some modifications to give fuller profiles through the transition region accompanied by an increase in the growth rate of the

boundary layer. In the low Reynolds number computation prediction, this modification was accomplished by shortening the transition region or zone somewhat unrealistically. Preferably, the eddy viscosity model could be altered as discussed by Bushnell and Morris (ref. 31) who show that in the low local Reynolds number inner portion of a hypersonic transitional boundary layer, the eddy viscosity can be very large. This increase in eddy viscosity accounts for the high intensity turbulent fluctuations which occur in the transition region (ref. 31). The growth of  $\delta^*$ ,  $\delta$ , and  $\theta$  should also be more pronounced if the modified eddy viscosity models of reference 31 are used.

### Leading-Edge Effects

The theoretical predictions of laminar  $\delta^*$  were 25 percent to 30 percent below the experimental values, whereas the predicted laminar momentum thickness was from 30 percent to 40 percent below experimental values. As previously discussed, the final predicted (fig. 12) and experimental values of  $\delta^*$  were matched at the last laminar profile survey station by extending the lengths of laminar flow in the calculations. At present, the source of the discrepancy between the former predicted and experimental values of  $\delta^*$  and  $\theta$  in the laminar flow region is not clear, but a possible cause may be the finite thickness of the leading edge. Because of the finite leading-edge thickness, the boundary layer near the leading edge develops under the influence of a detached curved shock (even for the small, 0.0051-cm, leading-edge thickness of the present investigation). A viscous-induced pressure gradient exists over the forward portion of the wedge as shown in figure 3. The distribution and magnitude of the pressure in the vicinity of the leading edge are unknown. Calculations indicated that the first survey station was downstream of the variable entropy region for each unit Reynolds number case. The free-stream Reynolds number based on leading-edge thickness varied from  $0.495 \times 10^3$  to  $2.52 \times 10^3$ .

Strong evidence supporting the conjecture that the finite leading-edge thickness can significantly affect the growth of  $\delta$ ,  $\delta^*$ , and  $\theta$  can be found in reference 27, where the leading-edge thickness of a flat plate at  $M_\infty = 3.05$  was increased from 0.00076 cm to 0.0150 cm and finally to 0.0297 cm. The effect of the change in leading-edge thickness from 0.00076 cm to 0.0150 cm was twofold: the laminar boundary-layer thickness increased by a factor of about 2, and the velocity profile decreased in slope near the wall (decrease in skin friction) while becoming less full in the outer part of the boundary layer. A further increase in leading-edge thickness from 0.0150 cm to 0.0297 cm produced no noticeable change in the velocity slope near the wall but did result in less profile fullness in the outer part of the boundary layer with an approximate 30-percent increase in the laminar boundary-layer thickness. The effect of small changes in leading-edge thickness on downstream velocity profile shape just described (from ref. 27) may have influenced the growth of  $\delta$ ,  $\delta^*$ , and  $\theta$  in the laminar boundary layer of the present investigation

in a similar manner. The results of reference 27 indicate that a slight increase in leading-edge thickness decreases the velocity slope near the wall at a downstream station and thus decreases the skin friction. Since for a two-dimensional shape with zero pressure gradient

$$\theta = \int_0^x \frac{C_f}{2} dx = \frac{\mu_w}{\rho_e u_e^2} \int_0^x \left( \frac{du}{dy} \right)_w dx$$

a decrease in  $C_f$  should produce a corresponding decrease in  $\theta$ . However, the corresponding increase in experimental boundary-layer thickness due to a finite leading-edge thickness would tend to increase the momentum thickness since the momentum thickness is proportional to the boundary-layer thickness for a given profile shape. Therefore, the net effect of leading-edge thickness on momentum thickness would be trade-off between these two opposing factors. This same reasoning would also apply to the displacement thickness; a reduction in the velocity profile slope near the wall due to a finite leading-edge thickness and a subsequent reduction in profile fullness in the outer part of the boundary layer together with an increase in boundary-layer thickness would tend to increase the experimental displacement thickness over the theoretical zero leading-edge thickness predicted displacement thickness.

## CONCLUSIONS

Detailed boundary-layer pitot surveys were obtained near adiabatic wall conditions on a  $5^\circ$  half-angle wedge placed at  $10^\circ$  incidence in a nominal Mach 20 helium free-stream flow with a local Mach number of about 6.5. The following conclusions can be made:

1. Mach number, density, and velocity profiles indicate that the boundary layer varied from laminar to fully turbulent along the wedge surface for all but the lowest of four unit Reynolds number test cases ( $R_e/cm = 0.056 \times 10^6$  to  $0.255 \times 10^6$ ).
2. Comparison of experimental Mach number, density, and velocity profiles at the lowest and highest unit Reynolds number test cases with profiles predicted by a finite-difference computation method indicated the need for improved eddy viscosity models to represent better the higher-intensity turbulent fluctuations which occur in the transition region.
3. Theoretical predictions of laminar displacement and momentum thickness were approximately 30 percent and 35 percent, respectively, below the corresponding experimental results. A possible source of this discrepancy may be the downstream effect of a finite leading-edge thickness on boundary-layer-profile shape and growth.

Langley Research Center,  
National Aeronautics and Space Administration,  
Hampton, Va., August 24, 1971.

## REFERENCES

1. Harris, Julius E.: Numerical Solution of the Equations for Compressible Laminar, Transitional, and Turbulent Boundary Layers and Comparisons With Experimental Data. NASA TR R-368, 1971.
2. Adams, John C., Jr.: Eddy Viscosity-Intermittency Factor Approach to Numerical Calculation of Transitional Heating on Sharp Cones in Hypersonic Flow. AEDC-TR-70-210, U.S. Air Force, Nov. 1970.
3. Bushnell, Dennis M.; and Beckwith, Ivan E.: Calculation of Nonequilibrium Hypersonic Turbulent Boundary Layers and Comparisons With Experimental Data. AIAA J., vol. 8, no. 8, Aug. 1970, pp. 1462-1469.
4. Smith, A. M. O.; and Cebeci, T.: Numerical Solution of the Turbulent-Boundary-Layer Equations. Rep. No. 33735 (Contract N0W 66-0324-c), Douglas Aircraft Co., Inc., May 29, 1967.
5. Herring, H. James; and Mellor, George L.: A Method of Calculating Compressible Turbulent Boundary Layers. NASA CR-1144, 1968.
6. Danberg, James E.: Characteristics of the Turbulent Boundary Layer With Heat and Mass Transfer: Data Tabulation. NOLTR-67-6, U.S. Navy, Jan. 23, 1967. (Available from DDC as AD 650 272.)
7. Danberg, James E.: Characteristics of the Turbulent Boundary Layer With Heat and Mass Transfer at  $M = 6.7$ . NOLTR-64-99, U.S. Navy, Oct. 19, 1964. (Available from DDC as AD 452 471.)
8. Kutschenreuter, Paul H., Jr.; Brown, David L.; Hoelmer, Werner; et al.: Investigation of Hypersonic Inlet Shock-Wave Boundary Layer Interaction. Pt. II - Continuous Flow Test and Analyses. AFFDL-TR-65-36, U.S. Air Force, Apr. 1966. (Available from DDC as AD 636 981.)
9. Deem, R. E.: Results of a Flat Plate Boundary Layer Transition Experiment at Mach 5 - Model: General. Rep. No. SM-47643 (Contract No. AF 33(657)-10660), Missile & Space Syst. Div., Douglas Aircraft Co., June 10, 1964.
10. Deem, R. E.: Results of a Flat Plate Boundary Layer Transition Experiment at Mach 8 - Model: General. Rep. No. SM-45918 (Contract No. AF 33(657)-10660), Missile & Space Syst. Div., Douglas Aircraft Co., Apr. 24, 1964. (Available from DDC as AD 805 547.)
11. Deem, R. E.: Results of a Flat Plate Boundary Layer Transition Experiment at Mach 10 - Model: General. Rep. No. SM-47630 (Contract No. AF 33(657)-10660), Missile & Space Syst. Div., Douglas Aircraft Co., May 22, 1964.

12. Korkegi, Robert H.: Transition Studies and Skin-Friction Measurements on an Insulated Flat Plate at a Mach Number of 5.8. *J. Aeronaut. Sci.*, vol. 23, no. 2, Feb. 1956, pp. 97-107, 192.
13. Adcock, Jerry B.; Peterson, John B., Jr.; and McRee, Donald I.: Experimental Investigation of a Turbulent Boundary Layer at Mach 6, High Reynolds Numbers, and Zero Heat Transfer. NASA TN D-2907, 1965.
14. Stroud, J. F.; and Miller, L. D.: An Experimental and Analytical Investigation of Hypersonic Inlet Boundary Layers. Vol. II. Data Reduction Program and Tabulated Experimental Data. AFFDL-TR-65-123-Vol. II, U.S. Air Force, Aug. 1965. (Available from DDC as AD 621 344.)
15. Samuels, Richard D.; Peterson, John B., Jr.; and Adcock, Jerry B.: Experimental Investigation of the Turbulent Boundary Layer at a Mach Number of 6 With Heat Transfer at High Reynolds Numbers. NASA TN D-3858, 1967.
16. Jones, Robert A.; and Feller, William V.: Preliminary Surveys of the Wall Boundary Layer in a Mach 6 Axisymmetric Tunnel. NASA TN D-5620, 1970.
17. Arrington, James P.; Joiner, Roy C., Jr.; and Henderson, Arthur, Jr.: Longitudinal Characteristics of Several Configurations at Hypersonic Mach Numbers in Conical and Contoured Nozzles. NASA TN D-2489, 1964.
18. Fischer, M. C.; Maddalon, D. V.; Weinstein, L. M.; and Wagner, R. D., Jr.: Boundary-Layer Pitot and Hot-Wire Surveys at  $M_\infty \approx 20$ . *AIAA J.*, vol. 9, no. 5, May 1971, pp. 826-834.
19. Beckwith, Ivan E.; Harvey, William D.; and Clark, Frank L. (With appendix A by Ivan E. Beckwith, William D. Harvey, and Christine M. Darden and appendix B by William D. Harvey, Lemuel E. Forrest, and Frank L. Clark): Comparisons of Turbulent-Boundary-Layer Measurements at Mach Number 19.5 With Theory and an Assessment of Probe Errors. NASA TN D-6192, 1971.
20. Erickson, Wayne D.: Real-Gas Correction Factors for Hypersonic Flow Parameters in Helium. NASA TN D-462, 1960.
21. Bertram, Mitchel H.: Hypersonic Laminar Viscous Interaction Effects on the Aerodynamics of Two-Dimensional Wedge and Triangular Planform Wings. NASA TN D-3523, 1966.
22. Bushnell, Dennis M.; Johnson, Charles B.; Harvey, William D.; and Feller, William V.: Comparison of Prediction Methods and Studies of Relaxation in Hypersonic Turbulent Nozzle-Wall Boundary Layers. NASA TN D-5433, 1969.
23. Maddalon, Dal V.; and Jackson, Willis E.: A Survey of the Transport Properties of Helium at High Mach Number Wind-Tunnel Conditions. NASA TM X-2020, 1970.

24. Johnson, Charles B.; and Bushnell, Dennis M.: Power-Law Velocity-Profile-Exponent Variations With Reynolds Number, Wall Cooling, and Mach Number in a Turbulent Boundary Layer. NASA TN D-5753, 1970.
25. Wagner, R. D., Jr.; Maddalon, D. V.; and Weinstein, L. M.: Influence of Measured Freestream Disturbances on Hypersonic Boundary-Layer Transition. AIAA J., vol. 8, no. 9, Sept. 1970, pp. 1664-1670.
26. Monaghan, R. J.: The Use of Pitot Tubes in the Measurement of Laminar Boundary Layers in Supersonic Flow. Papers Presented at the Seventh Meeting of the Wind Tunnel and Model Testing Panel (Ottawa), AGARD, June 1955, pp. 101-131. (Available from DDC as AD No. 109 913.)
27. Bradfield, W. S.; DeCoursin, D. G.; and Blumer, C. B.: The Effect of Leading-Edge Bluntness on a Laminar Supersonic Boundary Layer. J. Aeronaut. Sci., vol. 21, no. 6, June 1954, pp. 373-382, 398.
28. Blue, Robert E.; and Low, George M.: Factors Affecting Laminar Boundary Layer Measurements in a Supersonic Stream. NACA TN 2891, 1953.
29. O'Donnell, Robert M.: Experimental Investigation at a Mach Number of 2.41 of Average Skin-Friction Coefficients and Velocity Profiles for Laminar and Turbulent Boundary Layers and an Assessment of Probe Effects. NACA TN 3122, 1954.
30. Rotta, J. C.: Heat Transfer and Temperature Distribution in Turbulent Boundary Layers at Supersonic and Hypersonic Flow. Recent Developments in Boundary Layer Research, Pt. I, AGARDograph 97, May 1965, pp. 35-63.
31. Bushnell, D. M.; and Morris, D. J.: Eddy Viscosity Distributions in a Mach 20 Turbulent Boundary Layer. AIAA J., vol. 9, no. 4, Apr. 1971, pp. 764-766.

TABLE 1.- SUMMARY OF FREE-STREAM AND LOCAL TEST CONDITIONS AND  
COMPUTED BOUNDARY-LAYER PARAMETERS

$P_{t,\infty}$ MN/m <sup>2</sup>	$T_{t,\infty}$ °K	$M_\infty$	$M_e$ (average)	$R_\infty$ /cm	$R_e$ /cm (average)	x, cm	$\delta$ , cm	$\delta^*$ , cm	$\theta$ , cm	$R_{e,\theta}$
3.55	345	19.1	6.2	$0.097 \times 10^6$	$0.056 \times 10^6$	9.91	0.53	0.34	0.00879	$0.49 \times 10^3$
↓	↓	↓	↓	↓	↓	18.03	.66	.43	.01118	.63
↓	↓	↓	↓	↓	↓	22.86	.74	.49	.01222	.68
↓	↓	↓	↓	↓	↓	43.18	1.17	.63	.01847	1.03
↓	↓	↓	↓	↓	↓	48.26	1.60	.77	.02184	1.22
↓	↓	↓	↓	↓	↓	53.34	1.68	.78	.02352	1.32
↓	↓	↓	↓	↓	↓	59.94	1.88	.87	.02647	1.48
7.00	353	20.3	6.5	.178	.101	9.91	.46	.27	.00671	.68
↓	↓	↓	↓	↓	↓	18.03	.51	.34	.00899	.91
↓	↓	↓	↓	↓	↓	22.86	.53	.34	.00909	.92
↓	↓	↓	↓	↓	↓	43.18	.17	.54	.01638	1.65
↓	↓	↓	↓	↓	↓	48.26	1.37	.69	.02014	2.03
↓	↓	↓	↓	↓	↓	53.34	1.58	.72	.02167	2.19
↓	↓	↓	↓	↓	↓	59.94	1.70	.80	.02433	2.46
10.45	348	21.0	6.7	.263	.149	9.91	.43	.24	.00582	.87
↓	↓	↓	↓	↓	↓	18.03	.43	.26	.00711	1.06
↓	↓	↓	↓	↓	↓	22.86	.43	.26	.00716	1.07
↓	↓	↓	↓	↓	↓	43.18	1.32	.55	.01621	2.42
↓	↓	↓	↓	↓	↓	48.26	1.57	.69	.01920	2.86
↓	↓	↓	↓	↓	↓	53.34	1.52	.68	.02065	3.08
20.79	354	21.7	6.6	.495	.255	9.91	.31	.20	.00488	1.24
↓	↓	↓	↓	↓	↓	18.03	.38	.23	.00709	1.81
↓	↓	↓	↓	↓	↓	22.86	.61	.21	.00673	1.72
↓	↓	↓	↓	↓	↓	43.18	1.19	.48	.01612	4.11
↓	↓	↓	↓	↓	↓	48.26	1.45	.62	.01920	4.90
↓	↓	↓	↓	↓	↓	53.34	1.45	.64	.02136	5.45

TABLE 2.- TABULATED PROFILE DATA

(a)  $p_{t,\infty} = 3.55 \text{ MN/m}^2$

$y/\delta^*$	$P_{t,2}/(P_{t,2})_e$	$M/M_e$	$T_t/T_{t,\infty}$	$u/u_e$	$\rho/\rho_e$
$x = 9.91 \text{ cm}; M_e = 6.1; \delta^* = 0.34 \text{ cm}; (P_{t,2})_e = 36.82 \text{ kN/m}^2; P_w = 0.673 \text{ kN/m}^2; Re/cm = 0.054 \times 10^6$					
0.000	0.000	0.000	0.854	0.000	0.080
.158	.025	.115	.910	.386	.088
.219	.025	.115	.910	.386	.088
.354	.027	.123	.914	.411	.090
.467	.029	.136	.919	.447	.093
.588	.040	.175	.933	.543	.104
.678	.056	.219	.946	.633	.119
.746	.086	.280	.960	.729	.147
.821	.141	.366	.974	.822	.199
.867	.185	.423	.980	.863	.240
.927	.247	.492	.985	.900	.298
.950	.287	.531	.987	.917	.335
.980	.335	.575	.990	.932	.380
1.002	.387	.619	.992	.945	.429
1.032	.451	.669	.993	.957	.488
1.055	.522	.721	.995	.967	.555
1.085	.577	.758	.996	.973	.606
1.108	.649	.804	.997	.980	.672
1.138	.715	.844	.997	.985	.734
1.168	.781	.884	.998	.989	.797
1.191	.830	.910	.998	.992	.841
1.213	.881	.938	.999	.995	.890
1.259	.910	.954	.999	.996	.917
1.356	.959	.979	.999	.998	.962
1.470	.985	.993	.999	.999	.988
1.598	1.000	1.000	1.000	1.000	1.000
$x = 18.03 \text{ cm}; M_e = 6.1; \delta^* = 0.43 \text{ cm}; (P_{t,2})_e = 36.72 \text{ kN/m}^2; P_w = 0.662 \text{ kN/m}^2; Re/cm = 0.054 \times 10^6$					
0.000	0.000	0.000	0.857	0.000	0.079
.167	.022	.094	.903	.324	.084
.364	.028	.131	.919	.436	.091
.537	.045	.190	.939	.578	.108
.627	.066	.241	.953	.674	.128
.692	.087	.282	.962	.734	.147
.758	.121	.336	.970	.796	.179
.824	.165	.397	.978	.847	.220
.889	.225	.468	.984	.890	.276
.961	.312	.553	.989	.926	.357
.991	.370	.603	.991	.941	.411
1.027	.428	.650	.993	.953	.465
1.056	.483	.691	.994	.962	.515
1.092	.564	.748	.996	.972	.592
1.122	.624	.787	.996	.978	.648
1.164	.711	.840	.997	.985	.728
1.194	.787	.886	.998	.990	.800
1.230	.841	.915	.999	.993	.850
1.265	.901	.948	.999	.995	.907
1.301	.941	.968	.999	.997	.943
1.361	.974	.985	.999	.998	.974
1.546	1.000	1.000	1.000	1.000	1.000

TABLE 2.- TABULATED PROFILE DATA - Continued

(a)  $p_{t,\infty} = 3.55 \text{ MN/m}^2$  - Continued

$y/\delta^*$	$p_{t,2}/(p_{t,2})_e$	$M/M_e$	$T_t/T_{t,\infty}$	$u/u_e$	$\rho/\rho_e$
$x = 22.86 \text{ cm}; M_e = 6.2; \delta^* = 0.49 \text{ cm}; (p_{t,2})_e = 37.32 \text{ kN/m}^2; p_w = 0.659 \text{ kN/m}^2; R_e/cm = 0.056 \times 10^6$					
0.000	0.000	0.000	0.858	0.000	0.077
.171	.023	.103	.909	.357	.084
.331	.024	.111	.912	.379	.085
.460	.028	.129	.919	.434	.089
.589	.039	.175	.936	.550	.102
.672	.059	.225	.950	.650	.119
.765	.097	.299	.965	.758	.155
.806	.138	.362	.974	.822	.194
.843	.163	.395	.978	.848	.216
.884	.207	.449	.983	.882	.259
.925	.263	.507	.987	.910	.311
.967	.324	.564	.990	.931	.367
1.008	.416	.640	.993	.952	.452
1.049	.510	.722	.995	.968	.555
1.096	.594	.768	.996	.976	.620
1.137	.702	.836	.997	.984	.721
1.173	.794	.888	.998	.990	.805
1.220	.842	.916	.999	.993	.851
1.256	.903	.949	.999	.996	.907
1.308	.941	.969	.999	.997	.943
1.391	.983	.990	.999	.999	.982
1.478	1.000	1.000	1.000	1.000	1.000
$x = 43.18; M_e = 6.2; \delta^* = 0.63 \text{ cm}; (p_{t,2})_e = 35.49 \text{ kN/m}^2; p_w = 0.622 \text{ kN/m}^2; R_e/cm = 0.054 \times 10^6$					
0.000	0.000	0.000	0.869	0.000	0.078
.179	.027	.124	.923	.415	.089
.374	.068	.244	.958	.678	.129
.553	.119	.333	.973	.793	.177
.659	.179	.415	.981	.859	.233
.773	.237	.479	.986	.895	.286
.882	.310	.551	.990	.925	.355
.960	.388	.619	.992	.945	.428
1.033	.456	.672	.994	.958	.492
1.078	.511	.711	.995	.965	.542
1.110	.566	.749	.996	.972	.593
1.187	.665	.813	.997	.981	.686
1.261	.761	.871	.998	.988	.777
1.338	.830	.910	.999	.992	.841
1.464	.907	.951	.999	.996	.912
1.639	.963	.981	.999	.998	.965
1.923	.978	.989	.999	.999	.979
2.200	1.000	1.000	1.000	1.000	1.000

TABLE 2.- TABULATED PROFILE DATA - Continued

(a)  $p_{t,\infty} = 3.55 \text{ MN/m}^2$  - Continued

$y/\delta^*$	$p_{t,2}/(p_{t,2})_e$	$M/M_e$	$T_t/T_{t,\infty}$	$u/u_e$	$\rho/\rho_e$
$x = 48.26 \text{ cm}; M_e = 6.4; \delta^* = 0.77 \text{ cm}; (p_{t,2})_e = 37.26 \text{ kN/m}^2; p_w = 0.618 \text{ kN/m}^2; R_e/\text{cm} = 0.060 \times 10^6$					
0.000	0.000	0.000	0.873	0.000	0.074
.185	.030	.144	.934	.478	.090
.318	.038	.170	.942	.545	.098
.404	.082	.273	.966	.730	.139
.517	.137	.361	.978	.825	.191
.623	.188	.425	.983	.871	.238
.732	.255	.499	.988	.908	.301
.831	.319	.560	.991	.931	.361
.930	.397	.627	.993	.950	.436
1.010	.476	.687	.995	.963	.508
1.089	.546	.737	.996	.971	.575
1.169	.630	.792	.997	.979	.653
1.232	.697	.833	.998	.985	.716
1.325	.769	.876	.998	.989	.784
1.437	.846	.919	.999	.993	.855
1.540	.894	.945	.999	.995	.900
1.672	.933	.966	.999	.997	.938
1.785	.960	.980	.999	.998	.963
1.964	.981	.990	.999	.999	.983
2.116	1.000	1.000	1.000	1.000	1.000
$x = 53.34 \text{ cm}; M_e = 6.3; \delta^* = 0.78 \text{ cm}; (p_{t,2})_e = 36.67 \text{ kN/m}^2; p_w = 0.617 \text{ kN/m}^2; R_e/\text{cm} = 0.058 \times 10^6$					
0.000	0.000	0.000	0.878	0.000	0.075
.157	.031	.144	.936	.479	.091
.241	.053	.211	.954	.630	.112
.316	.094	.294	.970	.756	.151
.382	.131	.352	.977	.817	.186
.453	.167	.400	.982	.854	.219
.519	.194	.434	.984	.875	.245
.581	.224	.467	.987	.893	.273
.675	.260	.504	.989	.910	.307
.763	.304	.546	.991	.926	.347
.854	.364	.599	.993	.942	.404
.943	.416	.641	.994	.953	.452
1.024	.471	.684	.995	.962	.505
1.112	.540	.733	.996	.971	.569
1.177	.597	.771	.997	.976	.623
1.233	.646	.802	.997	.981	.668
1.314	.707	.838	.998	.985	.724
1.393	.769	.875	.998	.989	.783
1.484	.823	.906	.999	.992	.834
1.569	.864	.929	.999	.994	.873
1.673	.903	.949	.999	.996	.908
1.813	.949	.973	.999	.998	.952
1.937	.976	.987	.999	.999	.977
2.081	.990	.995	.999	.999	.991
2.218	1.000	1.000	1.000	1.000	1.000

TABLE 2.- TABULATED PROFILE DATA - Continued

(a)  $p_{t,\infty} = 3.55 \text{ MN/m}^2$  - Concluded

$y/\delta^*$	$p_{t,2}/(p_{t,2})_e$	$M/M_e$	$T_t/T_{t,\infty}$	$u/u_e$	$\rho/\rho_e$
$x = 59.94 \text{ cm}; M_e = 6.4; \delta^* = 0.87 \text{ cm}; (p_{t,2})_e = 37.14 \text{ kN/m}^2; p_w = 0.616 \text{ kN/m}^2; Re/cm = 0.059 \times 10^6$					
0.000	0.000	0.000	0.869	0.000	0.074
.132	.030	.144	.932	.479	.090
.246	.061	.231	.956	.667	.119
.316	.113	.325	.972	.792	.168
.418	.170	.424	.983	.871	.236
.506	.214	.457	.985	.889	.264
.579	.252	.496	.988	.908	.299
.687	.294	.537	.990	.924	.338
.804	.340	.580	.991	.937	.383
.918	.390	.621	.993	.949	.428
.982	.444	.664	.994	.958	.479
1.023	.509	.711	.995	.967	.540
1.158	.547	.737	.996	.972	.574
1.222	.613	.781	.997	.978	.637
1.310	.674	.820	.997	.983	.696
1.400	.737	.857	.998	.987	.753
1.511	.797	.892	.998	.991	.809
1.587	.861	.928	.999	.994	.871
1.716	.910	.954	.999	.996	.917
1.909	.971	.986	.999	.999	.974
2.125	1.000	1.000	1.000	1.000	1.000

TABLE 2.- TABULATED PROFILE DATA - Continued

(b)  $p_{t,\infty} = 7.00 \text{ MN/m}^2$

$y/\delta^*$	$P_{t,2}/(P_{t,2})_e$	$M/M_e$	$T_t/T_{t,\infty}$	$u/u_e$	$\rho/\rho_e$
$x = 9.91 \text{ cm}; M_e = 6.3; \delta^* = 0.27 \text{ cm}; (P_{t,2})_e = 63.50 \text{ kN/m}^2; p_w = 1.072 \text{ kN/m}^2; Re/cm = 0.094 \times 10^6$					
0.000	0.000	0.000	0.834	0.000	0.081
.209	.023	.101	.891	.344	.087
.313	.024	.107	.894	.362	.088
.446	.027	.123	.902	.408	.091
.589	.037	.165	.920	.518	.101
.665	.056	.225	.940	.642	.122
.741	.084	.275	.953	.721	.145
.760	.098	.301	.959	.755	.159
.807	.131	.351	.968	.807	.189
.855	.169	.403	.975	.849	.225
.912	.222	.465	.981	.887	.275
.931	.259	.503	.984	.905	.308
.950	.298	.540	.986	.920	.345
.978	.356	.592	.989	.937	.399
1.007	.408	.634	.991	.948	.446
1.035	.465	.678	.993	.958	.500
1.083	.595	.768	.995	.975	.621
1.111	.649	.803	.996	.980	.671
1.149	.704	.837	.997	.984	.723
1.168	.776	.879	.998	.989	.790
1.197	.840	.915	.998	.992	.850
1.225	.896	.945	.999	.995	.901
1.253	.937	.967	.999	.997	.940
1.310	.960	.979	.999	.998	.962
1.396	.978	.989	.999	.999	.979
1.481	.989	.993	.999	.999	.988
1.567	.996	.996	.999	.999	.994
1.690	1.000	1.000	1.000	1.000	1.000
$x = 18.03 \text{ cm}; M_e = 6.4; \delta^* = 0.34 \text{ cm}; (P_{t,2})_e = 62.40 \text{ kN/m}^2; p_w = 1.048 \text{ kN/m}^2; Re/cm = 0.096 \times 10^6$					
0.000	0.000	0.000	0.843	0.000	0.081
.237	.023	.099	.896	.339	.086
.371	.030	.138	.914	.450	.094
.438	.038	.169	.926	.527	.102
.519	.048	.198	.936	.592	.112
.623	.076	.261	.953	.702	.138
.690	.098	.300	.961	.754	.158
.734	.130	.350	.969	.807	.188
.808	.173	.408	.977	.853	.229
.838	.198	.438	.980	.872	.252
.875	.223	.466	.982	.887	.275
.905	.257	.502	.985	.905	.308
.942	.297	.539	.987	.920	.344
.979	.340	.579	.989	.933	.384
1.009	.383	.615	.991	.943	.424
1.038	.435	.657	.992	.954	.474
1.075	.495	.701	.994	.963	.529
1.105	.552	.740	.995	.970	.581
1.142	.616	.784	.996	.977	.643
1.179	.693	.830	.997	.983	.713
1.201	.746	.862	.998	.987	.762
1.231	.824	.907	.998	.992	.836
1.268	.905	.951	.999	.996	.912
1.305	.948	.973	.999	.997	.951
1.342	.972	.985	.999	.998	.974
1.379	.985	.992	.999	.999	.985
1.483	1.000	1.000	1.000	1.000	1.000

TABLE 2.- TABULATED PROFILE DATA - Continued

(b)  $p_{t,\infty} = 7.00 \text{ MN/m}^2$  - Continued

$y/\delta^*$	$P_{t,2}/(P_{t,2})_e$	$M/M_e$	$T_t/T_{t,\infty}$	$u/u_e$	$\rho/\rho_e$
$x = 22.86 \text{ cm}; M_e = 6.3; \delta^* = 0.34 \text{ cm}; (p_{t,2})_e = 61.67 \text{ kN/m}^2; p_w = 1.040 \text{ kN/m}^2; R_e/\text{cm} = 0.094 \times 10^6$					
0.000	0.000	0.000	0.853	0.000	0.080
.233	.024	.110	.907	.371	.088
.428	.038	.169	.930	.529	.102
.533	.054	.213	.944	.622	.117
.630	.083	.276	.959	.723	.145
.683	.104	.310	.965	.766	.164
.753	.127	.346	.971	.803	.186
.788	.167	.400	.977	.847	.223
.840	.209	.450	.982	.879	.262
.893	.260	.503	.986	.905	.309
.945	.322	.563	.989	.958	.368
.998	.398	.627	.992	.947	.439
1.050	.483	.692	.994	.961	.518
1.111	.574	.755	.996	.973	.602
1.163	.679	.822	.997	.982	.700
1.208	.742	.860	.998	.987	.759
1.253	.823	.907	.998	.992	.836
1.313	.900	.948	.999	.995	.906
1.366	.942	.970	.999	.997	.945
1.418	.971	.985	.999	.998	.974
1.516	.998	1.000	1.000	1.000	1.000
1.628	1.000	1.000	1.000	1.000	1.000
$x = 43.18 \text{ cm}; M_e = 6.6; \delta^* = 0.54 \text{ cm}; (p_{t,2})_e = 62.86 \text{ kN/m}^2; p_w = 0.986 \text{ kN/m}^2; R_e/\text{cm} = 0.103 \times 10^6$					
0.000	0.000	0.000	0.859	0.000	0.076
.211	.046	.195	.943	.594	.107
.328	.100	.304	.967	.766	.157
.432	.158	.388	.978	.844	.211
.530	.208	.450	.983	.883	.259
.633	.257	.500	.987	.907	.304
.751	.310	.552	.989	.927	.355
.845	.367	.602	.991	.942	.407
.920	.419	.643	.993	.953	.455
.985	.467	.680	.994	.961	.501
1.070	.534	.728	.995	.969	.563
1.140	.590	.766	.996	.975	.616
1.225	.649	.803	.997	.981	.670
1.300	.704	.837	.997	.985	.722
1.370	.763	.872	.998	.989	.778
1.450	.809	.898	.998	.991	.821
1.576	.871	.932	.999	.994	.878
1.759	.923	.960	.999	.996	.927
2.008	.959	.978	.999	.998	.960
2.351	.987	.993	.999	.999	.988
2.585	1.000	1.000	1.000	1.000	1.000

TABLE 2.- TABULATED PROFILE DATA - Continued

(b)  $P_{t,\infty} = 7.00 \text{ MN/m}^2$  - Continued

$y/\delta^*$	$P_{t,2}/(P_{t,2})_e$	$M/M_e$	$T_t/T_{t,\infty}$	$u/u_e$	$\rho/\rho_e$
$x = 48.26 \text{ cm}; M_e = 6.7; \delta^* = 0.69 \text{ cm}; (P_{t,2})_e = 65.60 \text{ kN/m}^2; p_w = 0.979 \text{ kN/m}^2; R_e/\text{cm} = 0.107 \times 10^6$					
0.000	0.000	0.000	0.853	0.000	0.074
.206	.051	.208	.945	.628	.110
.352	.072	.255	.957	.708	.129
.437	.146	.373	.976	.838	.198
.529	.204	.445	.983	.885	.253
.628	.257	.501	.986	.911	.302
.742	.311	.554	.989	.930	.354
.841	.370	.605	.991	.945	.409
.947	.426	.650	.993	.956	.462
1.039	.487	.695	.994	.965	.518
1.127	.555	.743	.996	.973	.583
1.208	.620	.786	.997	.979	.645
1.292	.683	.825	.997	.984	.703
1.373	.751	.866	.998	.988	.767
1.454	.803	.894	.998	.991	.814
1.538	.850	.921	.999	.994	.860
1.619	.886	.941	.999	.995	.894
1.711	.920	.959	.999	.997	.925
1.828	.948	.974	.999	.998	.953
1.957	.971	.984	.999	.998	.972
2.111	.988	.993	.999	.999	.988
2.284	1.000	1.000	1.000	1.000	1.000
$x = 53.34 \text{ cm}; M_e = 6.7; \delta^* = 0.72 \text{ cm}; (P_{t,2})_e = 65.70 \text{ kN/m}^2; p_w = 0.977 \text{ kN/m}^2; R_e/\text{cm} = 0.109 \times 10^6$					
0.000	0.000	0.000	0.864	0.000	0.073
.162	.046	.203	.948	.621	.107
.246	.073	.256	.960	.711	.129
.320	.123	.341	.974	.812	.177
.390	.169	.404	.981	.861	.220
.464	.217	.460	.985	.893	.265
.563	.268	.512	.988	.916	.313
.672	.312	.554	.990	.931	.354
.777	.351	.589	.992	.941	.391
.876	.397	.626	.993	.951	.433
.978	.450	.668	.994	.960	.484
1.087	.511	.712	.995	.968	.540
1.157	.563	.748	.996	.974	.589
1.238	.612	.781	.997	.979	.636
1.326	.689	.829	.997	.984	.708
1.414	.740	.859	.998	.988	.755
1.498	.788	.887	.998	.990	.802
1.586	.837	.914	.999	.993	.847
1.688	.886	.941	.999	.995	.894
1.840	.934	.965	.999	.997	.936
2.008	.970	.985	.999	.998	.972
2.156	.981	.991	.999	.999	.983
2.318	.991	.995	.999	.999	.991
2.533	1.000	1.000	1.000	1.000	1.000

TABLE 2. - TABULATED PROFILE DATA - Continued

(b)  $p_{t,\infty} = 7.00 \text{ MN/m}^2$  - Concluded

$y/\delta^*$	$P_{t,2}/(P_{t,2})_e$	$M/M_e$	$T_t/T_{t,\infty}$	$u/u_e$	$\rho/\rho_e$
$x = 59.94 \text{ cm}; M_e = 6.7; \delta^* = 0.80 \text{ cm}; (P_{t,2})_e = 65.03 \text{ kN/m}^2; P_w = 0.974 \text{ kN/m}^2; Re/cm = 0.106 \times 10^6$					
0.000	0.000	0.000	0.850	0.000	0.074
.141	.041	.180	.935	.569	.100
.221	.061	.233	.950	.672	.120
.268	.094	.296	.964	.762	.151
.310	.128	.348	.972	.816	.182
.368	.166	.400	.978	.856	.218
.422	.199	.440	.982	.881	.249
.495	.240	.484	.985	.903	.287
.569	.275	.520	.987	.918	.320
.668	.309	.551	.989	.929	.352
.783	.354	.590	.991	.941	.394
.889	.405	.633	.992	.952	.442
.965	.446	.664	.993	.959	.480
1.048	.489	.697	.994	.965	.522
1.109	.535	.729	.995	.971	.564
1.176	.572	.753	.996	.974	.597
1.263	.623	.787	.996	.979	.646
1.342	.676	.821	.997	.983	.696
1.432	.745	.861	.998	.988	.760
1.521	.799	.893	.998	.991	.811
1.636	.863	.929	.999	.994	.873
1.755	.903	.950	.999	.996	.909
1.918	.956	.977	.999	.998	.958
2.087	.981	.989	.999	.999	.980
2.289	.990	.995	.999	.999	.991
2.544	1.000	1.000	1.000	1.000	1.000

TABLE 2. - TABULATED PROFILE DATA - Continued

(c)  $p_{t,\infty} = 10.45 \text{ MN/m}^2$

$y/\delta^*$	$P_{t,2}/(P_{t,2})_e$	$M/M_e$	$T_t/T_{t,\infty}$	$u/u_e$	$\rho/\rho_e$
$x = 9.91 \text{ cm}; M_e = 6.5; \delta^* = 0.24 \text{ cm}; (p_{t,2})_e = 92.60 \text{ kN/m}^2; p_w = 1.478 \text{ kN/m}^2; Re/cm = 0.148 \times 10^6$					
0.000	0.000	0.000	0.857	0.000	0.080
.229	.021	.087	.899	.299	.084
.354	.022	.090	.901	.311	.085
.458	.025	.112	.911	.378	.088
.604	.039	.171	.933	.533	.103
.708	.063	.234	.951	.659	.126
.781	.092	.291	.963	.742	.153
.802	.116	.329	.969	.785	.175
.833	.149	.376	.975	.829	.206
.875	.182	.418	.979	.859	.237
.906	.227	.469	.984	.889	.278
.948	.297	.522	.987	.913	.327
.979	.365	.600	.991	.939	.407
1.010	.429	.650	.993	.952	.466
1.042	.510	.710	.995	.965	.541
1.073	.582	.760	.996	.973	.610
1.104	.663	.812	.997	.981	.685
1.135	.737	.856	.998	.986	.753
1.177	.802	.894	.998	.990	.815
1.208	.888	.941	.999	.995	.895
1.250	.945	.971	.999	.997	.948
1.323	.963	.981	.999	.998	.965
1.427	.978	.988	.999	.999	.979
1.542	.991	.993	.999	.999	.988
1.666	.999	.998	.999	.999	.997
1.739	1.000	1.000	1.000	1.000	1.000
$x = 18.03 \text{ cm}; M_e = 6.5; \delta^* = 0.26 \text{ cm}; (p_{t,2})_e = 88.40 \text{ kN/m}^2; p_w = 1.420 \text{ kN/m}^2; Re/cm = 0.141 \times 10^6$					
0.000	0.000	0.000	0.857	0.000	0.081
.274	.026	.119	.913	.396	.090
.401	.042	.180	.935	.551	.106
.518	.069	.246	.953	.677	.132
.567	.086	.281	.961	.728	.148
.626	.105	.312	.966	.767	.166
.675	.126	.344	.971	.800	.185
.724	.157	.387	.976	.836	.213
.782	.187	.424	.980	.863	.242
.831	.234	.477	.984	.892	.285
.880	.271	.515	.987	.909	.320
.929	.306	.548	.988	.922	.353
.958	.370	.605	.991	.940	.413
1.017	.412	.638	.992	.949	.451
1.056	.481	.690	.994	.961	.515
1.105	.534	.728	.995	.968	.565
1.144	.615	.781	.996	.976	.640
1.193	.672	.818	.997	.981	.694
1.232	.738	.857	.998	.986	.755
1.281	.810	.898	.998	.991	.822
1.320	.868	.930	.999	.994	.875
1.359	.924	.960	.999	.996	.928
1.418	.966	.982	.999	.998	.968
1.496	.988	.993	.999	.999	.988
1.584	1.000	1.000	1.000	1.000	1.000

TABLE 2.- TABULATED PROFILE DATA - Continued

(c)  $p_{t,\infty} = 10.45 \text{ MN/m}^2$  - Continued

$y/\delta^*$	$p_{t,2}/(p_{t,2})_e$	$M/M_e$	$T_t/T_{t,\infty}$	$u/u_e$	$\rho/\rho_e$
$x = 22.86 \text{ cm}; M_e = 6.5; \delta^* = 0.26 \text{ cm}; (p_{t,2})_e = 86.73 \text{ kN/m}^2; P_w = 1.405 \text{ kN/m}^2; R_e/\text{cm} = 0.137 \times 10^6$					
0.000	0.000	0.000	0.851	0.000	0.081
.313	.029	.135	.917	.440	.094
.401	.045	.191	.936	.574	.110
.460	.061	.229	.947	.648	.125
.538	.082	.273	.958	.717	.145
.607	.108	.318	.966	.772	.169
.685	.139	.363	.972	.817	.198
.754	.184	.422	.979	.860	.240
.822	.226	.468	.983	.887	.278
.901	.286	.530	.987	.915	.335
.950	.366	.601	.990	.939	.409
1.028	.441	.661	.993	.954	.479
1.106	.542	.734	.995	.969	.573
1.165	.623	.787	.996	.977	.649
1.253	.739	.859	.998	.986	.757
1.312	.843	.917	.998	.993	.854
1.390	.927	.962	.999	.996	.931
1.459	.984	.992	.999	.999	.985
1.605	1.000	1.000	1.000	1.000	1.000
$x = 43.18 \text{ cm}; M_e = 6.8; \delta^* = 0.55 \text{ cm}; (p_{t,2})_e = 91.20 \text{ kN/m}^2; P_w = 1.350 \text{ kN/m}^2; R_e/\text{cm} = 0.151 \times 10^6$					
0.000	0.000	0.000	0.851	0.000	0.075
.219	.054	.216	.946	.640	.113
.293	.083	.276	.960	.735	.141
.359	.129	.350	.972	.817	.183
.424	.172	.407	.979	.861	.224
.498	.219	.462	.984	.892	.268
.568	.255	.500	.986	.909	.302
.643	.295	.539	.988	.924	.340
.717	.334	.574	.990	.936	.375
.792	.380	.613	.992	.947	.419
.871	.415	.641	.993	.953	.452
.946	.455	.672	.994	.960	.489
1.029	.503	.706	.995	.967	.534
1.067	.543	.735	.995	.971	.572
1.150	.591	.767	.996	.976	.617
1.234	.650	.805	.997	.981	.672
1.313	.714	.844	.997	.986	.732
1.388	.770	.876	.998	.989	.783
1.467	.799	.901	.998	.992	.826
1.514	.826	.909	.998	.992	.838
1.593	.850	.925	.999	.994	.867
1.737	.896	.947	.999	.996	.904
1.882	.923	.960	.999	.997	.928
2.105	.949	.974	.999	.998	.952
2.380	.972	.986	.999	.999	.974
2.757	1.000	1.000	1.000	1.000	1.000

TABLE 2.- TABULATED PROFILE DATA - Continued

(c)  $P_{t,\infty} = 10.45 \text{ MN/m}^2$  - Concluded

$y/\delta^*$	$P_{t,2}/(P_{t,2})_e$	$M/M_e$	$T_t/T_{t,\infty}$	$u/u_e$	$\rho/\rho_e$
$x = 48.26 \text{ cm}; M_e = 6.9; \delta^* = 0.69 \text{ cm}; (P_{t,2})_e = 95.70 \text{ kN/m}^2; P_w = 1.338 \text{ kN/m}^2; R_e/\text{cm} = 0.164 \times 10^6$					
0.000	0.000	0.000	0.859	0.000	0.070
.218	.057	.224	.953	.687	.113
.340	.078	.267	.962	.733	.132
.381	.114	.327	.972	.803	.166
.432	.149	.377	.978	.846	.198
.480	.181	.418	.982	.873	.229
.532	.210	.450	.984	.891	.255
.580	.243	.486	.987	.908	.286
.647	.282	.525	.989	.923	.323
.717	.315	.556	.990	.934	.354
.787	.350	.587	.992	.943	.387
.861	.385	.616	.993	.950	.420
.931	.424	.646	.994	.957	.455
1.001	.469	.681	.994	.964	.499
1.071	.510	.710	.995	.969	.537
1.112	.548	.737	.996	.973	.573
1.167	.590	.765	.996	.977	.612
1.241	.638	.795	.997	.981	.657
1.286	.681	.822	.997	.984	.697
1.356	.733	.853	.998	.988	.745
1.419	.777	.878	.998	.990	.786
1.496	.815	.900	.998	.992	.822
1.581	.875	.933	.999	.995	.880
1.692	.914	.953	.999	.996	.914
1.825	.947	.970	.999	.998	.945
1.969	.969	.982	.999	.998	.967
2.099	.986	.991	.999	.999	.983
2.283	1.000	1.000	1.000	1.000	1.000
$x = 53.34 \text{ cm}; M_e = 6.8; \delta^* = 0.68 \text{ cm}; (P_{t,2})_e = 92.30 \text{ kN/m}^2; P_w = 1.335 \text{ kN/m}^2; R_e/\text{cm} = 0.155 \times 10^6$					
0.000	0.000	0.000	0.857	0.000	0.073
.134	.052	.212	.948	.637	.110
.228	.064	.237	.954	.682	.121
.269	.094	.295	.966	.764	.149
.340	.134	.357	.975	.826	.187
.403	.171	.405	.980	.861	.220
.471	.202	.442	.983	.884	.250
.534	.238	.482	.986	.904	.285
.613	.280	.523	.988	.920	.322
.695	.321	.562	.990	.933	.362
.788	.364	.599	.992	.944	.402
.874	.401	.629	.993	.952	.436
.971	.443	.662	.994	.959	.476
1.050	.490	.696	.995	.965	.520
1.117	.533	.727	.995	.971	.561
1.191	.586	.763	.996	.976	.611
1.262	.630	.792	.997	.980	.652
1.345	.680	.822	.997	.984	.697
1.397	.723	.849	.998	.987	.739
1.449	.756	.868	.998	.989	.770
1.505	.793	.889	.998	.991	.805
1.576	.839	.914	.999	.993	.847
1.658	.876	.935	.999	.995	.883
1.744	.915	.955	.999	.996	.918
1.871	.946	.971	.999	.998	.947
2.002	.963	.980	.999	.998	.964
2.133	.987	.992	.999	.999	.986
2.271	1.000	1.000	1.000	1.000	1.000

TABLE 2.- TABULATED PROFILE DATA - Continued

(d)  $p_{t,\infty} = 20.79 \text{ MN/m}^2$

$y/\delta^*$	$p_{t,2}/(p_{t,2})_e$	$M/M_e$	$T_t/T_{t,\infty}$	$u/u_e$	$\rho/\rho_e$
$x = 9.91 \text{ cm}; M_e = 6.6; \delta^* = 0.20 \text{ cm}; (p_{t,2})_e = 162.7 \text{ kN/m}^2; p_w = 2.564 \text{ kN/m}^2; Re/cm = 0.261 \times 10^6$					
0.000	0.000	0.000	0.850	0.000	0.085
.290	.022	.086	.893	.289	.088
.403	.023	.088	.894	.297	.089
.491	.027	.118	.908	.385	.094
.554	.032	.146	.919	.461	.100
.630	.041	.177	.930	.537	.109
.680	.054	.213	.941	.610	.121
.731	.079	.266	.955	.700	.144
.781	.108	.316	.964	.764	.171
.844	.156	.386	.974	.830	.216
.869	.215	.457	.981	.877	.271
.907	.251	.495	.984	.897	.305
.932	.304	.547	.987	.919	.355
.970	.361	.597	.990	.935	.407
.982	.415	.641	.992	.948	.457
1.008	.475	.686	.993	.958	.512
1.045	.543	.735	.995	.968	.576
1.083	.583	.760	.995	.972	.612
1.108	.642	.799	.996	.978	.667
1.171	.725	.851	.997	.985	.746
1.222	.828	.909	.998	.991	.840
1.272	.923	.961	.999	.996	.929
1.323	.961	.980	.999	.998	.964
1.348	.979	.988	.999	.999	.979
1.486	1.000	1.000	1.000	1.000	1.000
$x = 18.03 \text{ cm}; M_e = 6.5; \delta^* = 0.23 \text{ cm}; (p_{t,2})_e = 157.2 \text{ kN/m}^2; p_w = 2.483 \text{ kN/m}^2; Re/cm = 0.247 \times 10^6$					
0.000	0.000	0.000	0.843	0.000	0.086
.318	.048	.196	.933	.574	.116
.406	.077	.262	.951	.692	.144
.483	.100	.303	.960	.746	.165
.582	.130	.350	.968	.797	.193
.669	.162	.394	.974	.834	.223
.757	.206	.446	.979	.870	.263
.834	.258	.501	.984	.898	.311
.933	.325	.566	.988	.925	.375
1.021	.399	.628	.991	.944	.442
1.076	.483	.691	.993	.959	.519
1.174	.586	.762	.995	.972	.615
1.251	.678	.821	.997	.981	.700
1.339	.838	.915	.998	.992	.851
1.438	.947	.972	.999	.997	.949
1.515	.978	.988	.999	.999	.979
1.602	.991	.996	.999	.999	.994
1.690	1.000	1.000	1.000	1.000	1.000

TABLE 2.- TABULATED PROFILE DATA - Continued

(d)  $P_{t,\infty} = 20.79 \text{ MN/m}^2$  - Continued

$y/\delta^*$	$P_{t,2}/(P_{t,2})_e$	$M/M_e$	$T_t/T_{t,\infty}$	$u/u_e$	$\rho/\rho_e$
$x = 22.86 \text{ cm}; M_e = 6.5; \delta^* = 0.21 \text{ cm}; (P_{t,2})_e = 152.6 \text{ kN/m}^2; p_w = 2.475 \text{ kN/m}^2; R_e/\text{cm} = 0.239 \times 10^6$					
0.000	0.000	0.000	0.841	0.000	0.088
.352	.074	.256	.948	.677	.142
.364	.100	.303	.959	.743	.166
.412	.125	.343	.966	.786	.190
.497	.158	.389	.972	.827	.220
.582	.191	.430	.977	.857	.251
.667	.233	.476	.981	.884	.289
.764	.275	.518	.984	.904	.328
.861	.328	.568	.987	.924	.378
.946	.391	.622	.990	.941	.437
1.043	.457	.673	.992	.954	.497
1.116	.547	.737	.994	.967	.580
1.201	.632	.793	.996	.976	.659
1.286	.712	.842	.997	.983	.733
1.370	.822	.904	.998	.991	.833
1.467	.882	.939	.999	.994	.891
1.552	.925	.962	.999	.996	.931
1.746	.953	.977	.999	.998	.958
2.086	.977	.988	.999	.999	.979
2.426	.989	.995	.999	.999	.990
2.947	1.000	1.000	1.000	1.000	1.000
$x = 43.18 \text{ cm}; M_e = 6.6; \delta^* = 0.48 \text{ cm}; (P_{t,2})_e = 154.2 \text{ kN/m}^2; p_w = 2.420 \text{ kN/m}^2; R_e/\text{cm} = 0.246 \times 10^6$					
0.000	0.000	0.000	0.842	0.000	0.087
.240	.068	.243	.946	.661	.135
.320	.095	.295	.958	.736	.161
.395	.128	.347	.967	.794	.191
.443	.156	.385	.972	.827	.216
.528	.208	.448	.979	.871	.265
.597	.247	.491	.983	.893	.301
.667	.293	.536	.986	.913	.344
.715	.332	.572	.988	.926	.381
.784	.373	.606	.990	.937	.418
.864	.425	.648	.991	.949	.467
.981	.465	.678	.993	.956	.502
1.083	.517	.717	.994	.964	.552
1.152	.562	.747	.995	.969	.594
1.221	.612	.780	.996	.975	.640
1.280	.658	.809	.996	.979	.683
1.360	.716	.845	.997	.984	.737
1.429	.754	.866	.997	.987	.770
1.499	.796	.891	.998	.989	.810
1.568	.842	.917	.998	.992	.853
1.637	.875	.934	.999	.994	.884
1.744	.917	.957	.999	.996	.923
1.920	.950	.973	.999	.997	.952
2.064	.967	.983	.999	.998	.970
2.219	.982	.991	.999	.999	.985
2.331	.996	.998	.999	.999	.997
2.480	1.000	1.000	1.000	1.000	1.000

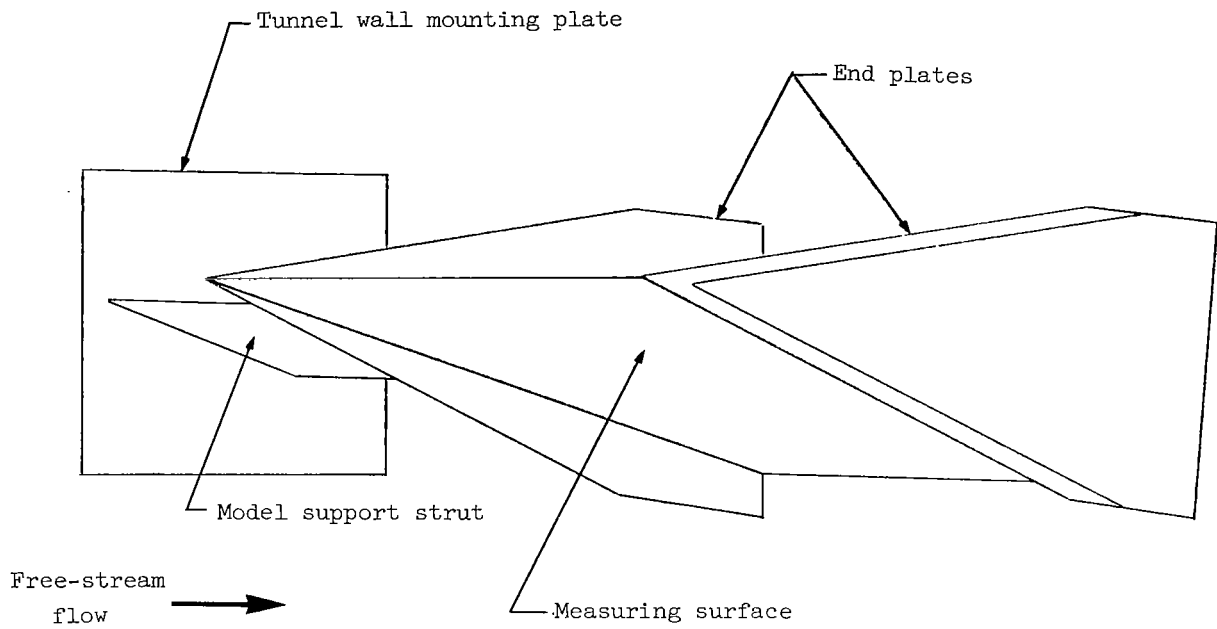
TABLE 2.- TABULATED PROFILE DATA - Concluded

(d)  $P_{t,\infty} = 20.79 \text{ MN/m}^2$  - Concluded

$y/\delta^*$	$P_{t,2}/(P_{t,2})_e$	$M/M_e$	$T_t/T_{t,\infty}$	$u/u_e$	$\rho/\rho_e$
$x = 48.26 \text{ cm}; M_e = 6.8; \delta^* = 0.62 \text{ cm}; (P_{t,2})_e = 166.5 \text{ kN/m}^2; P_w = 2.406 \text{ kN/m}^2; R_e/\text{cm} = 0.277 \times 10^6$					
0.000	0.000	0.000	0.854	0.000	0.079
.245	.066	.240	.952	.671	.128
.356	.083	.276	.960	.725	.145
.438	.125	.343	.971	.802	.183
.519	.174	.409	.978	.855	.229
.581	.216	.457	.983	.884	.268
.638	.255	.500	.986	.904	.305
.724	.312	.554	.989	.926	.358
.818	.352	.589	.990	.937	.395
.904	.404	.632	.992	.949	.444
.965	.446	.665	.993	.956	.484
1.030	.490	.698	.994	.963	.525
1.084	.530	.726	.995	.968	.562
1.153	.581	.760	.996	.974	.610
1.227	.636	.795	.996	.979	.659
1.284	.683	.825	.997	.983	.704
1.353	.742	.859	.998	.987	.757
1.431	.787	.885	.998	.990	.800
1.501	.835	.912	.998	.992	.844
1.607	.886	.940	.999	.995	.893
1.717	.921	.959	.999	.996	.926
1.832	.948	.973	.999	.997	.951
1.975	.967	.982	.999	.998	.968
2.143	.986	.993	.999	.999	.988
2.335	1.000	1.000	1.000	1.000	1.000
$x = 53.34 \text{ cm}; M_e = 6.7; \delta^* = 0.64 \text{ cm}; (P_{t,2})_e = 160.6 \text{ kN/m}^2; P_w = 2.399 \text{ kN/m}^2; R_e/\text{cm} = 0.261 \times 10^6$					
0.000	0.000	0.000	0.846	0.000	0.083
.178	.059	.225	.944	.639	.124
.296	.081	.270	.955	.710	.144
.383	.118	.333	.967	.787	.179
.481	.166	.399	.975	.843	.223
.560	.207	.448	.980	.875	.262
.635	.250	.494	.984	.899	.302
.734	.296	.538	.987	.917	.344
.821	.336	.575	.989	.930	.382
.904	.381	.613	.991	.942	.424
.983	.431	.653	.992	.952	.470
1.046	.475	.686	.993	.959	.512
1.121	.532	.726	.995	.967	.563
1.172	.574	.755	.995	.972	.603
1.239	.622	.786	.996	.977	.648
1.302	.669	.815	.997	.981	.690
1.365	.722	.848	.997	.985	.742
1.421	.771	.877	.998	.988	.787
1.484	.816	.901	.998	.991	.826
1.547	.853	.923	.999	.993	.864
1.618	.900	.947	.999	.995	.905
1.705	.933	.965	.999	.997	.936
1.807	.966	.982	.999	.998	.967
1.946	.984	.992	.999	.999	.985
2.096	.997	.998	.999	.999	.997
2.257	1.000	1.000	1.000	1.000	1.000

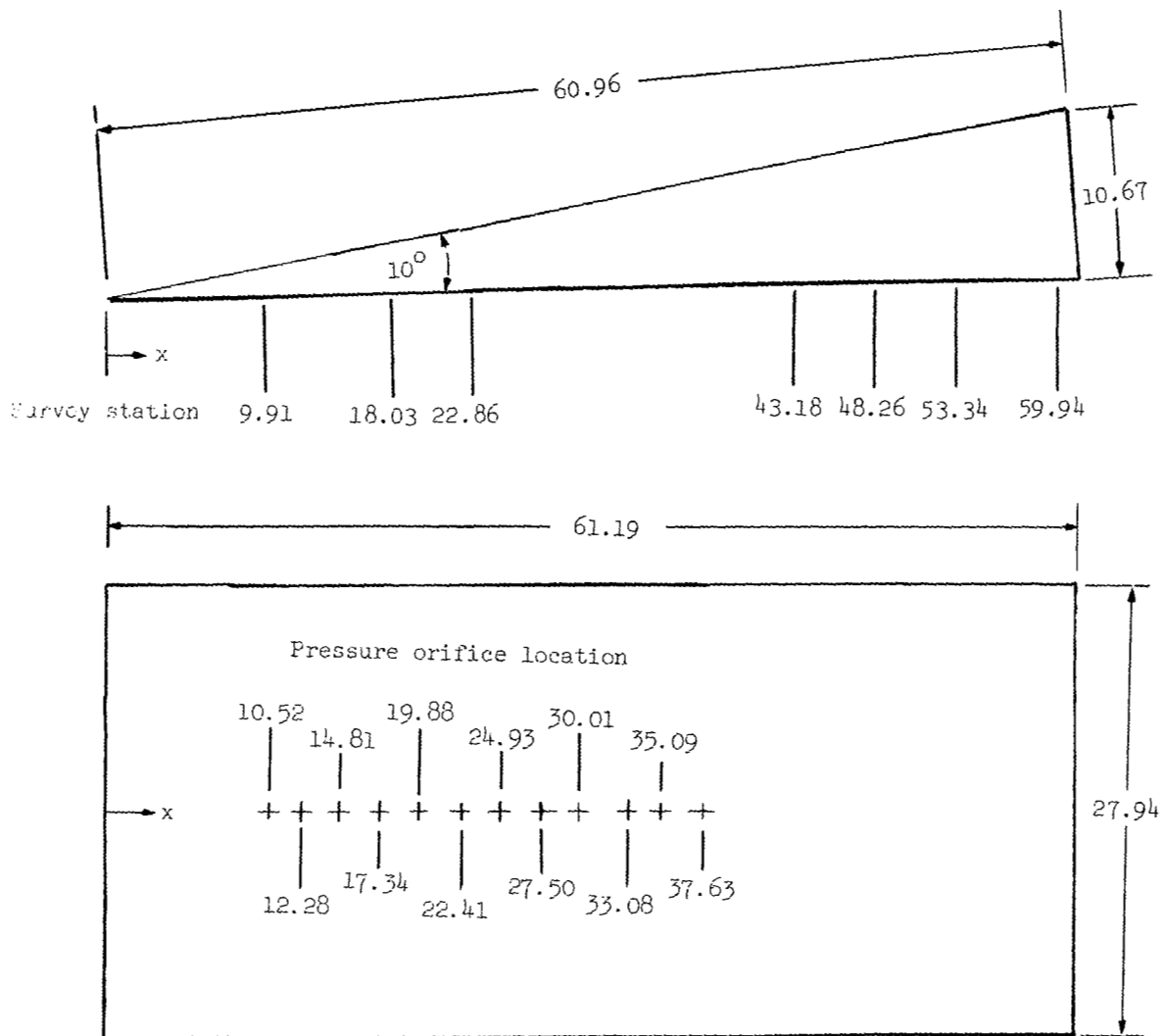
TABLE 3.- INPUT FOR THE FINITE-DIFFERENCE COMPUTATION  
METHOD OF HARRIS (REF. 1)

Parameter	Case 1 $Re/cm \approx 0.056 \times 10^6$	Case 2 $Re/cm \approx 0.255 \times 10^6$
$M_\infty$ . . . . .	19.1	21.7
$Me,i$ . . . . .	6.2	6.6
$\rho_{e,i}/\rho_\infty$ . . . . .	3.58	3.65
$T_{e,i}/T_\infty$ . . . . .	8.93	10.6
$p_e/p_\infty$ . . . . .	Figure 3	Figure 3
$T_{t,\infty}$ °K . . . . .	345	354
$N_{Pr}$ . . . . .	0.688	0.688
$N_{Pr,t}$ . . . . .	$0.95 [1 - 0.5(y/\delta)^2]$ or 1.0	$0.95 [1 - 0.5(y/\delta)^2]$ or 1.0
$p_{t,\infty}$ MN/m <sup>2</sup> . . . . .	3.55	20.79
$\epsilon$ , deg . . . . .	15.5	14.6
$x_{S,tr}$ , cm (ref. 25) . . . . .	25.40	11.69
$x_{E,tr}$ , cm (ref. 25) . . . . .	34.3 or 61.0	33.3



(a) Model mounted in tunnel.

Figure 1.- Sketch of basic wedge model.



(b) Pitot- and static-pressure measuring stations. Dimensions are in cm.  
 Figure 1.- Concluded.

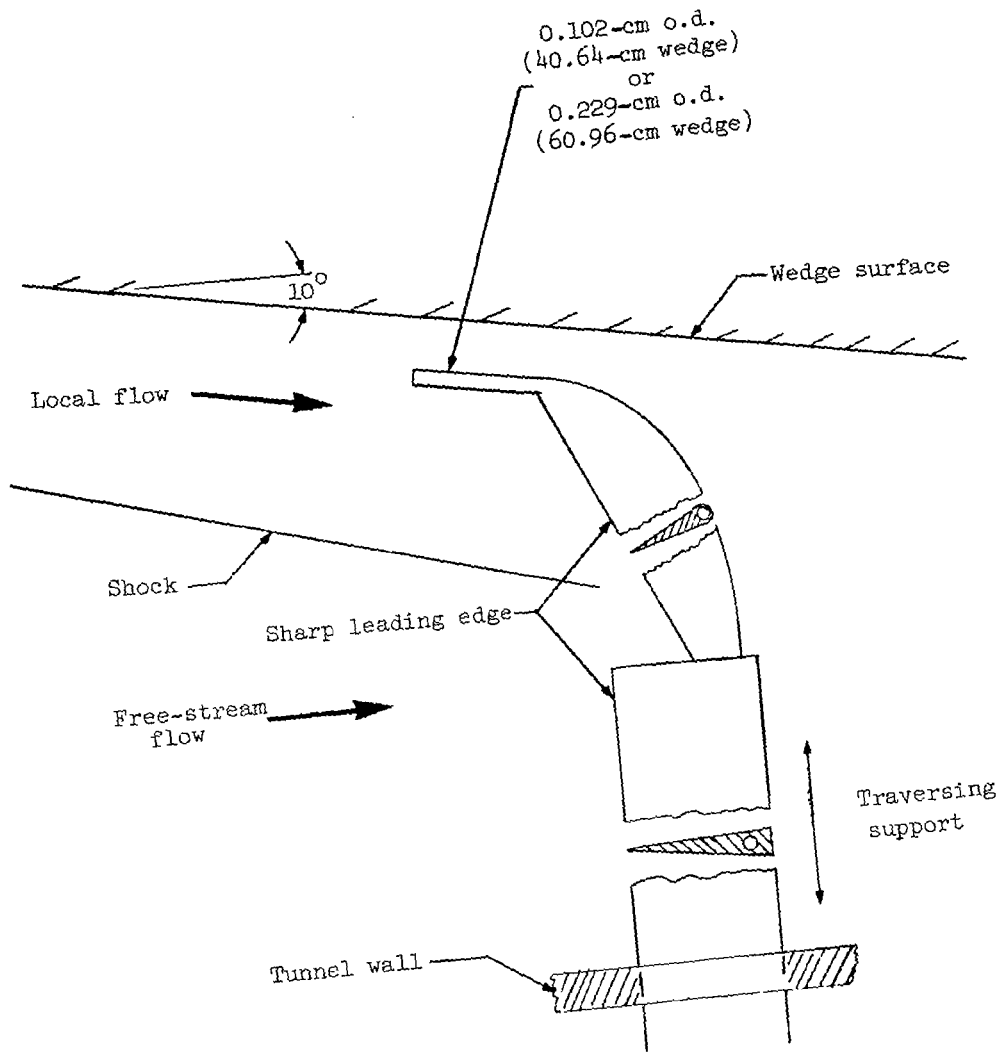


Figure 2.- Sketch of survey apparatus.

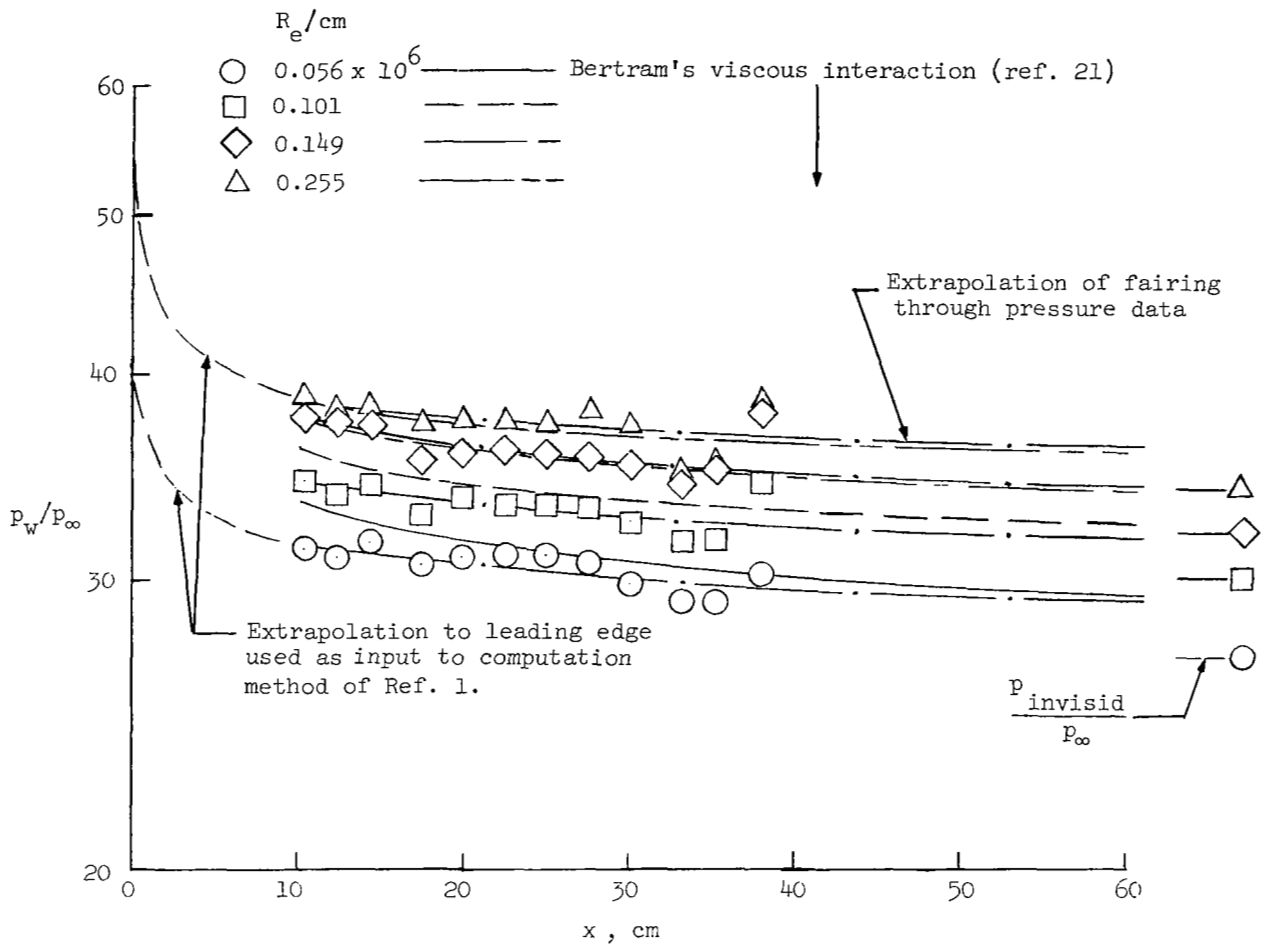
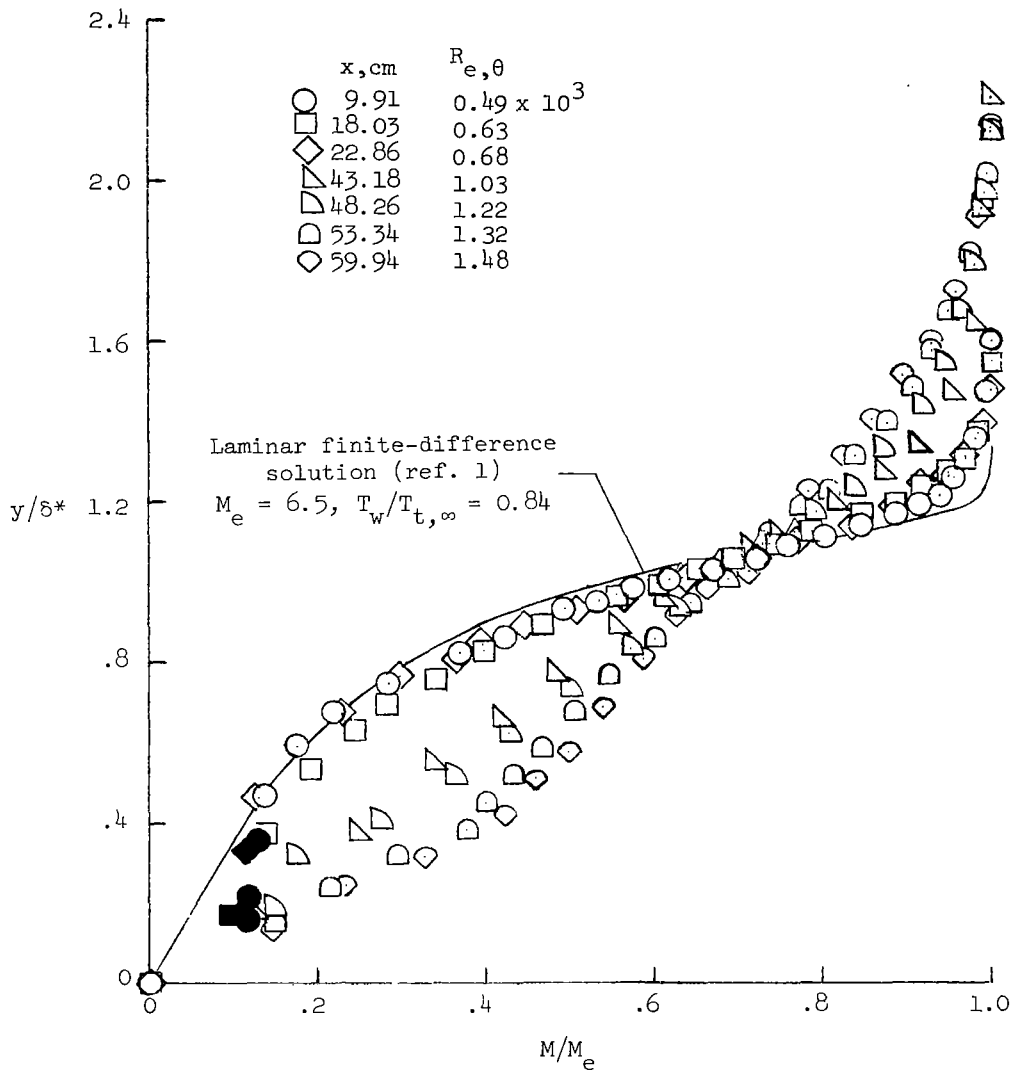
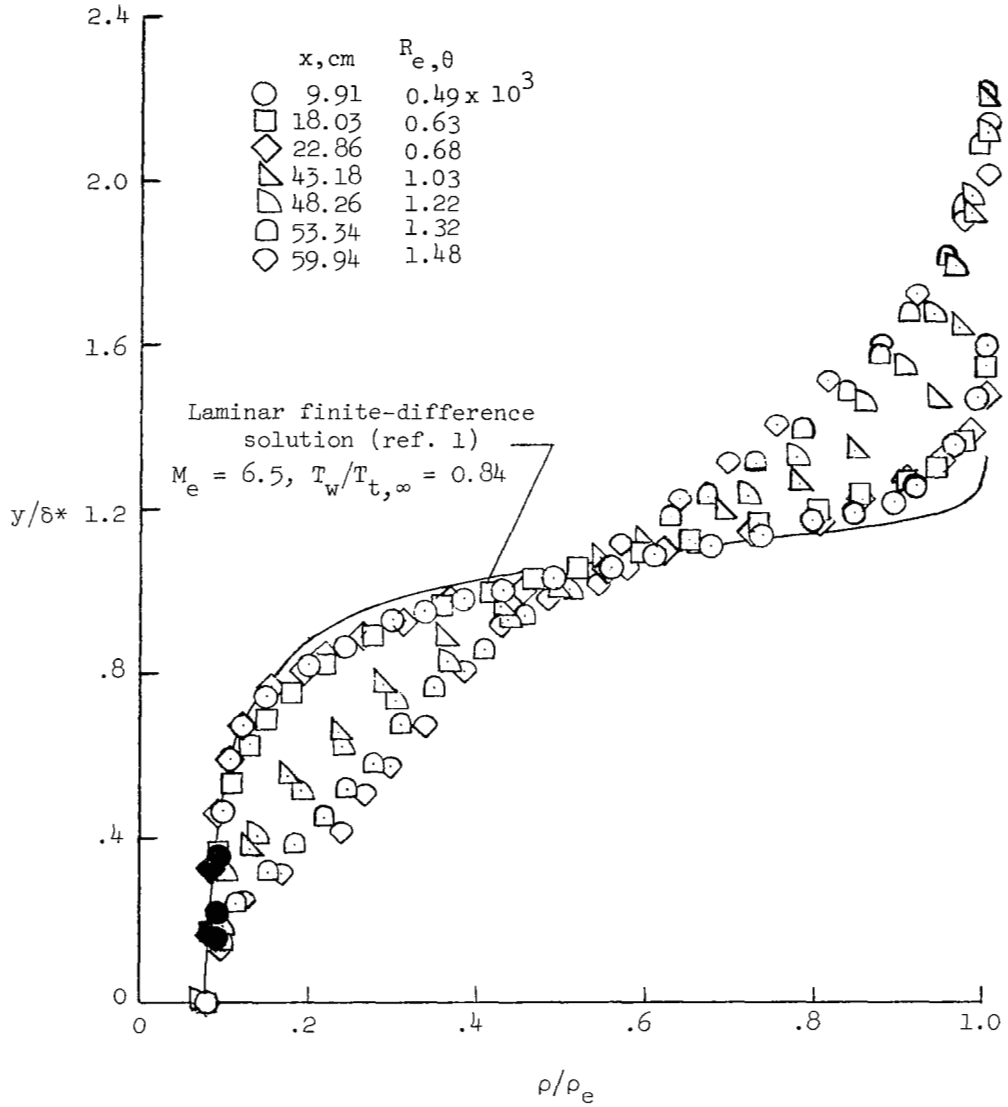


Figure 3.- Measured pressure distribution.



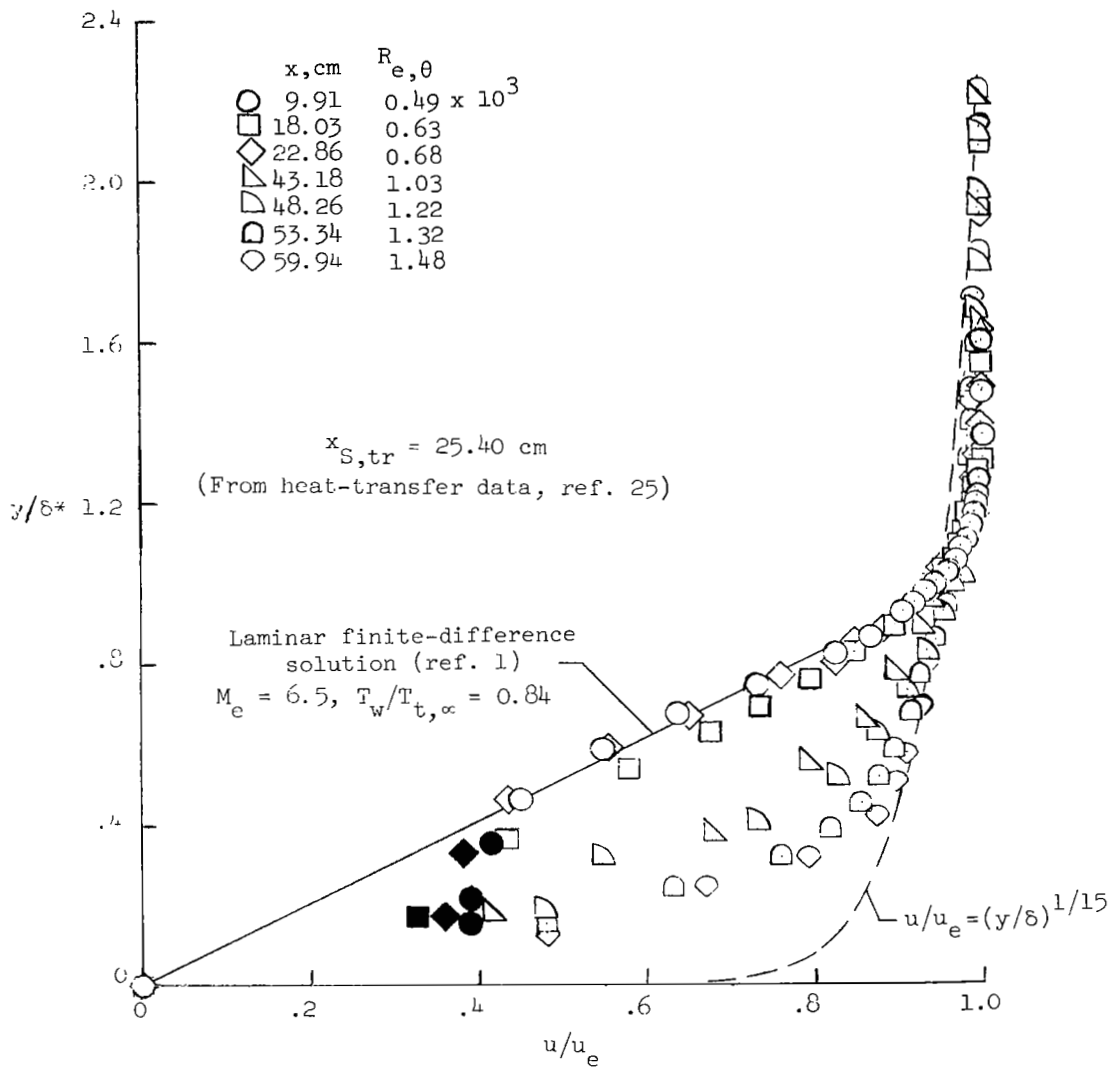
(a) Mach number profiles.

Figure 4.- Measured boundary-layer profiles at  $R_{e/cm} = 0.056 \times 10^6$ . Solid symbols represent data possibly distorted by wall.



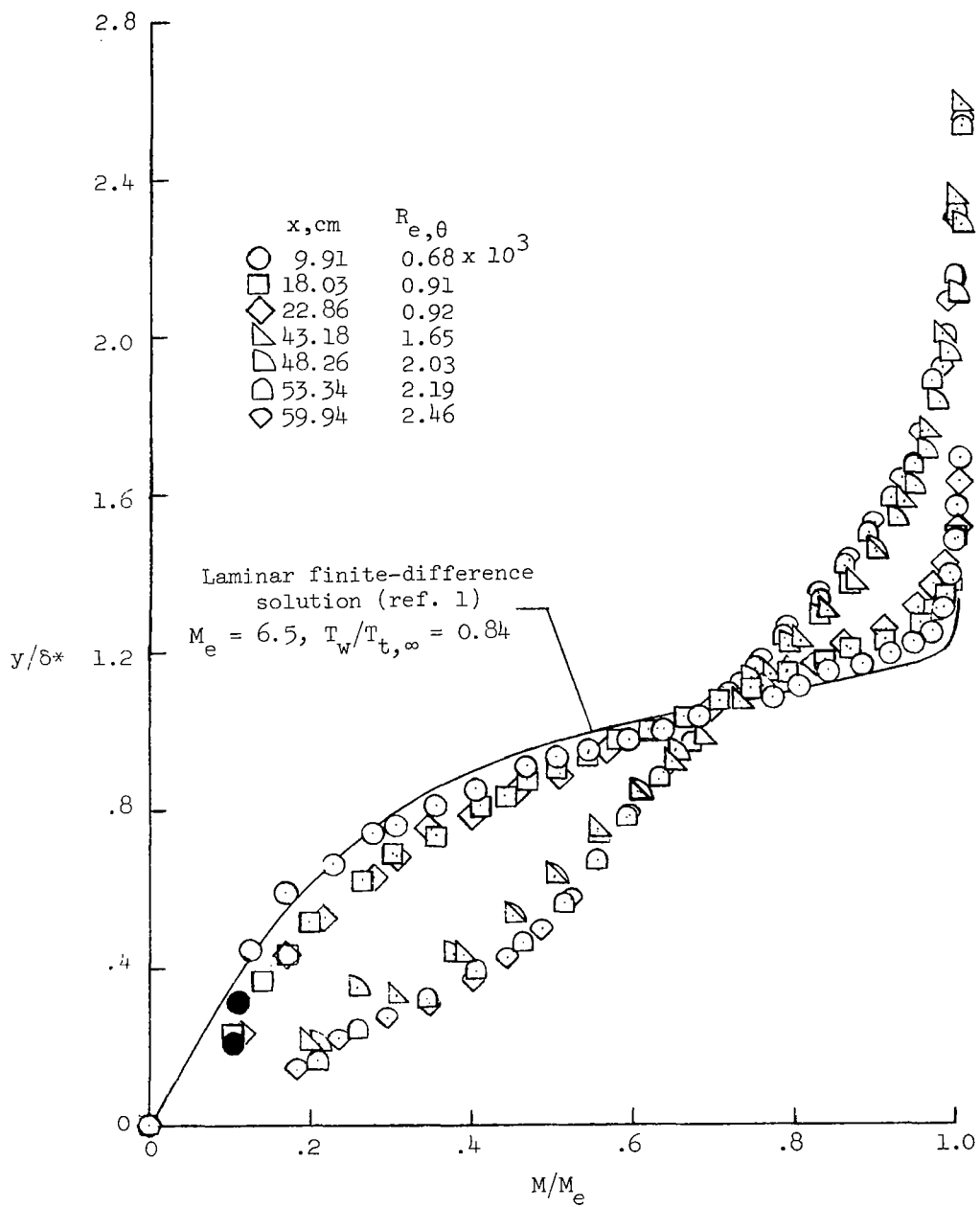
(b) Density profiles.

Figure 4. - Continued.



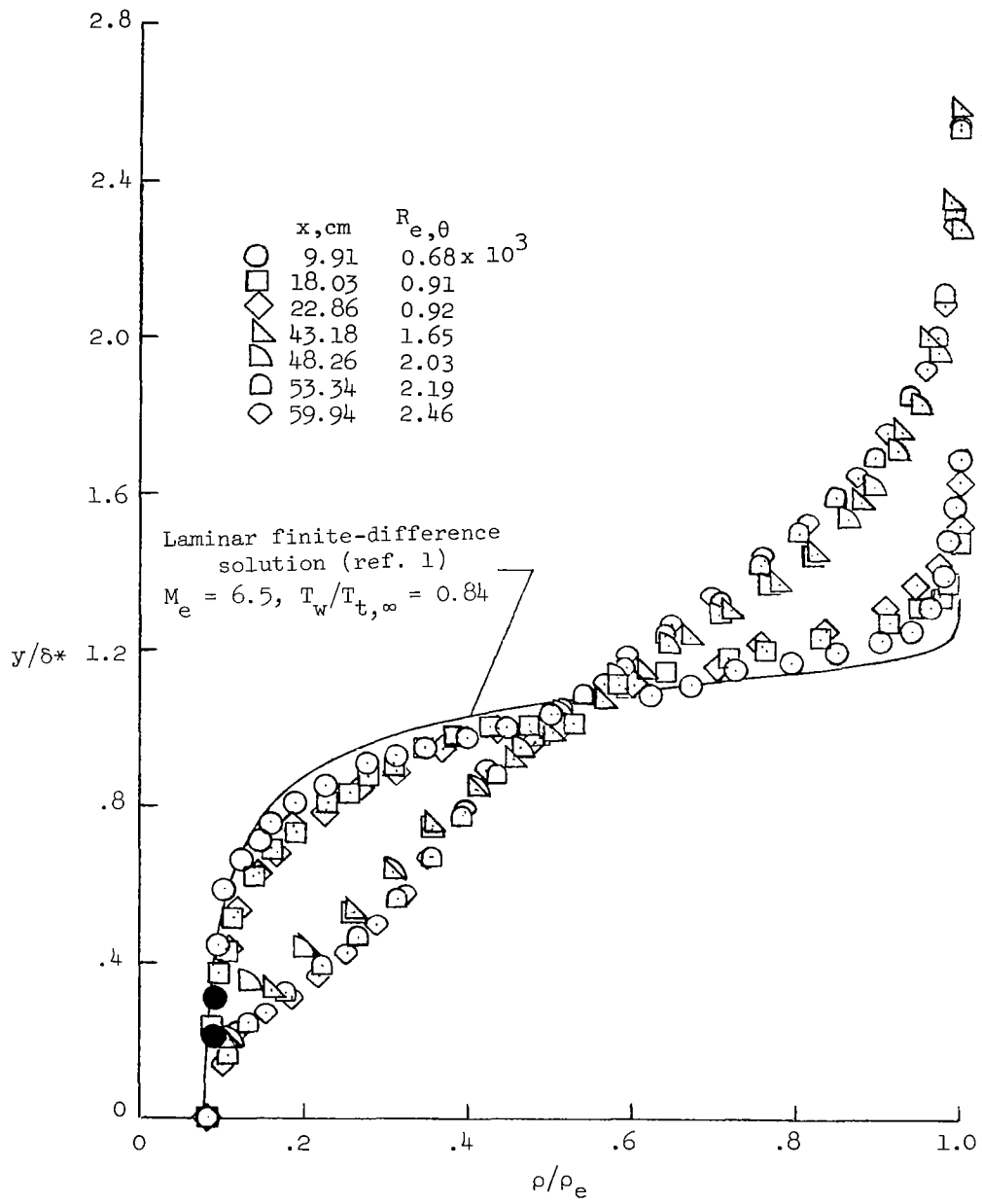
(c) Velocity profiles.

Figure 4.- Concluded.



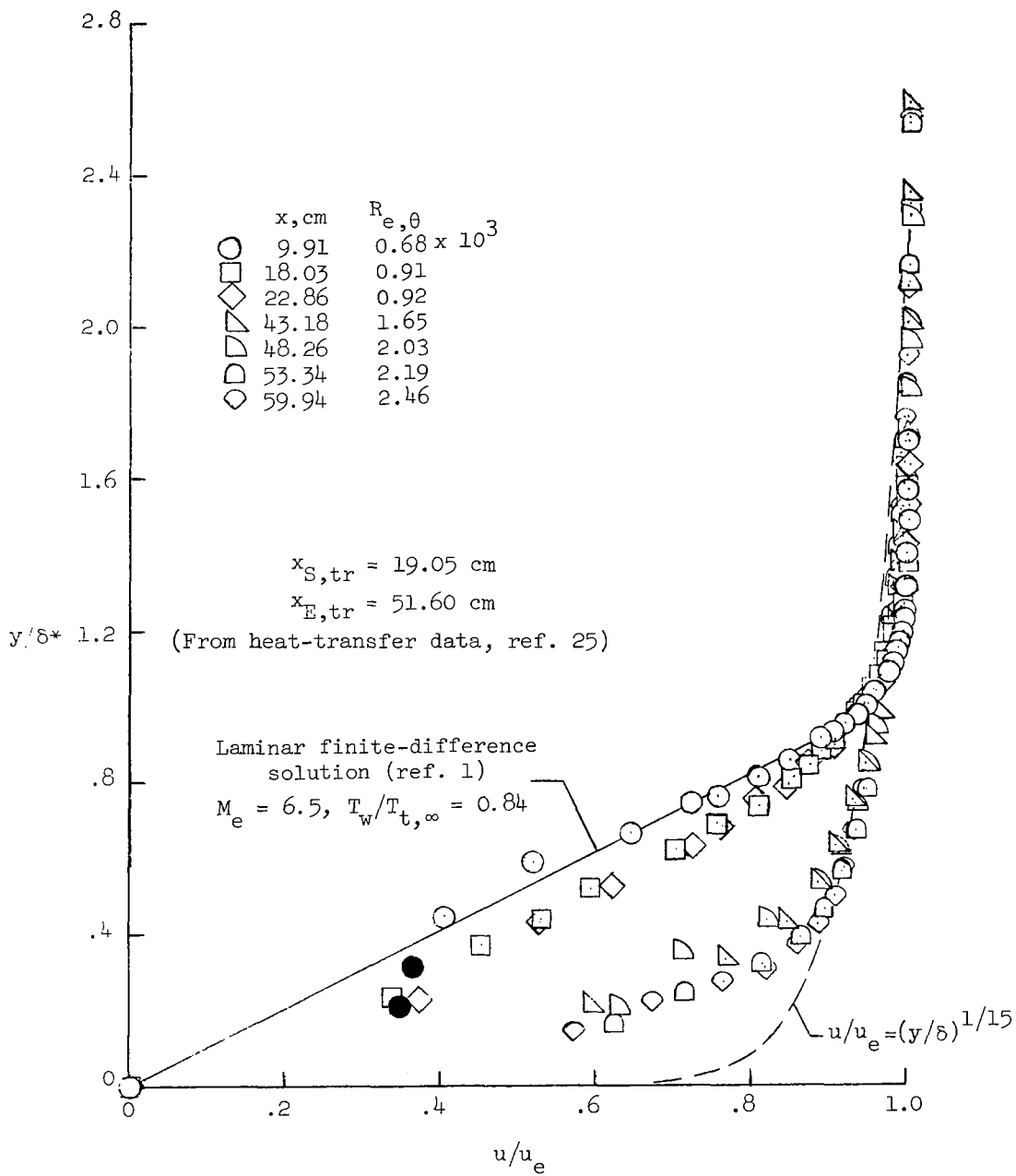
(a) Mach number profiles.

Figure 5.- Measured boundary-layer profiles at  $Re_\theta/cm = 0.101 \times 10^6$ . Solid symbols represent data possibly distorted by wall.



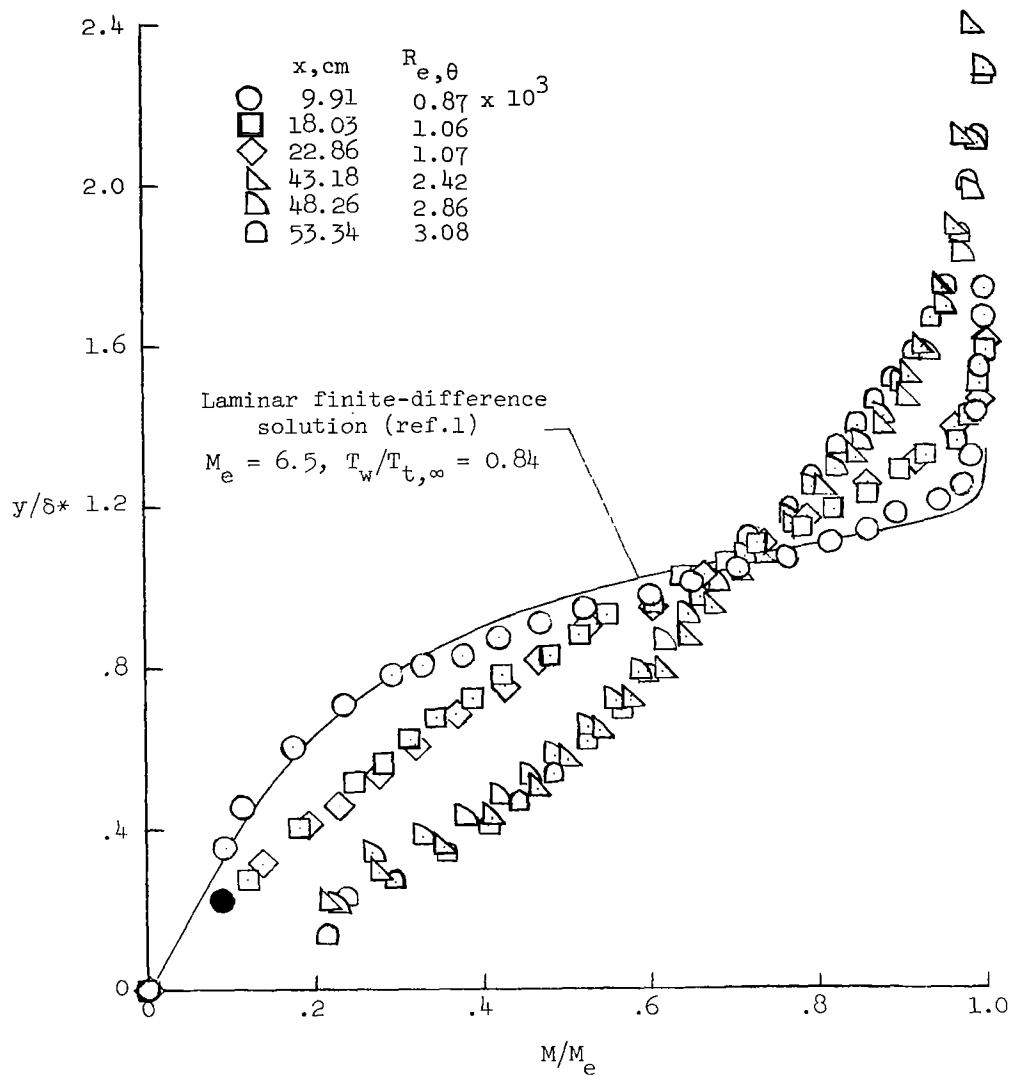
(b) Density profiles.

Figure 5.- Continued.



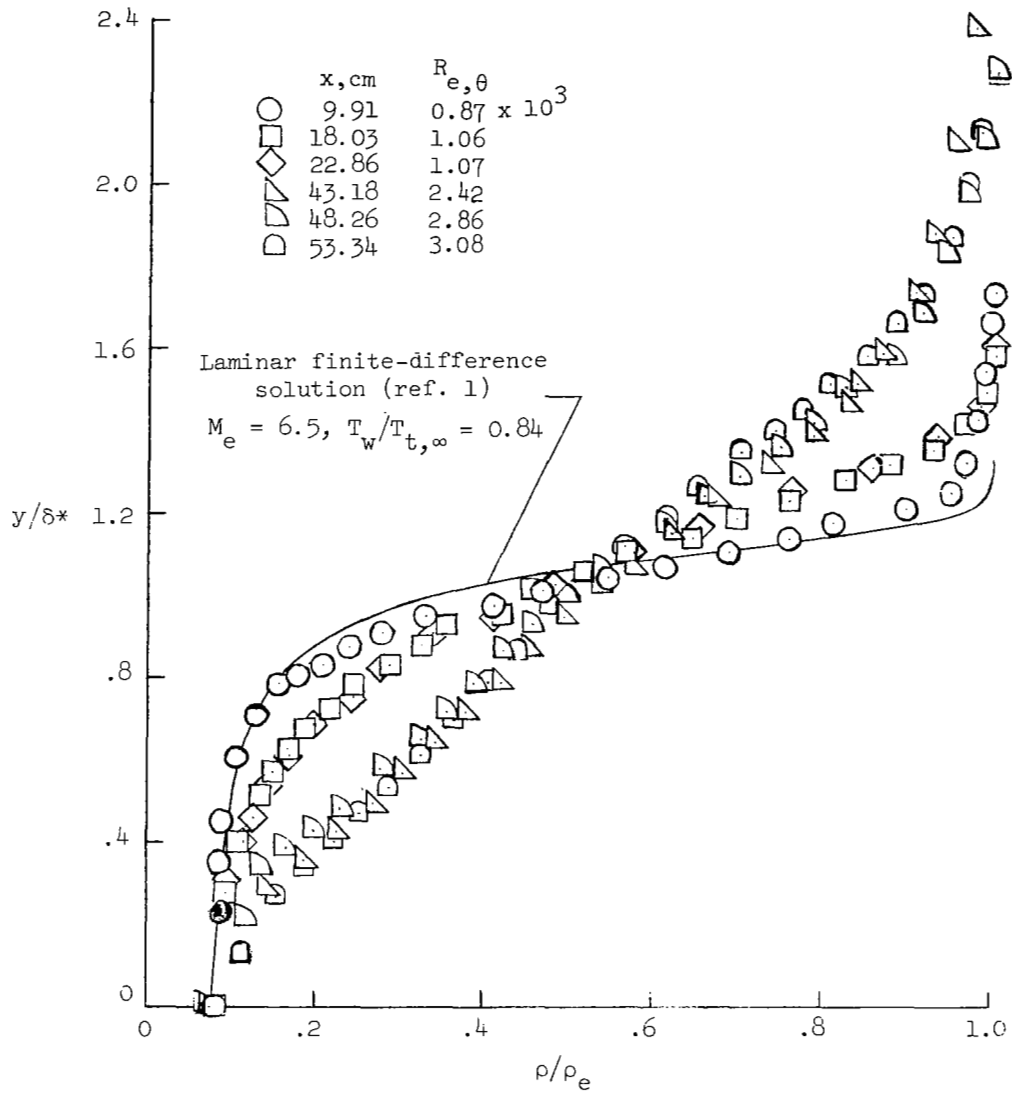
(c) Velocity profiles.

Figure 5.- Concluded.



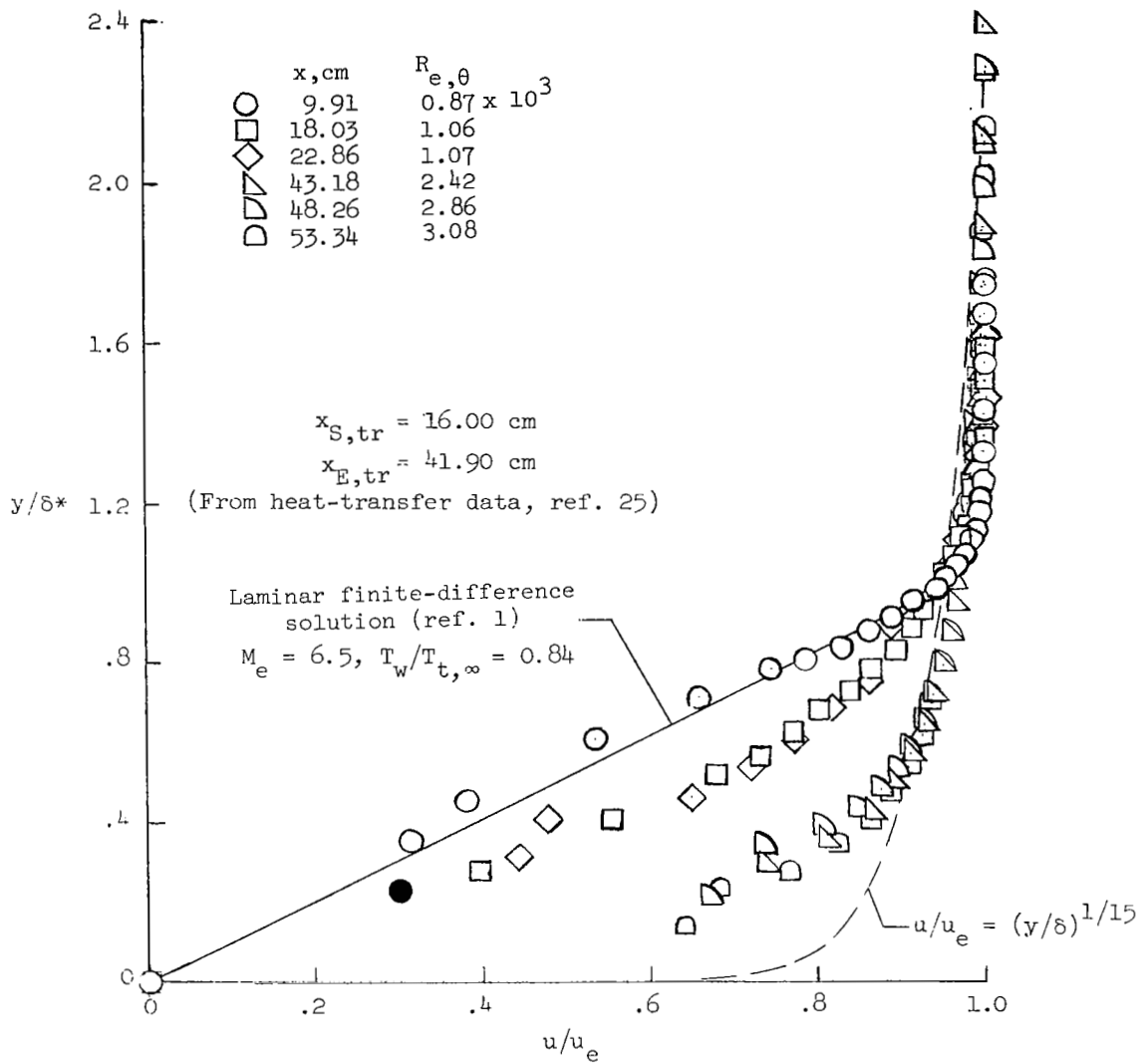
(a) Mach number profiles.

Figure 6.- Measured boundary-layer profiles at  $Re_e/cm = 0.149 \times 10^6$ . Solid symbols represent data possibly distorted by wall.



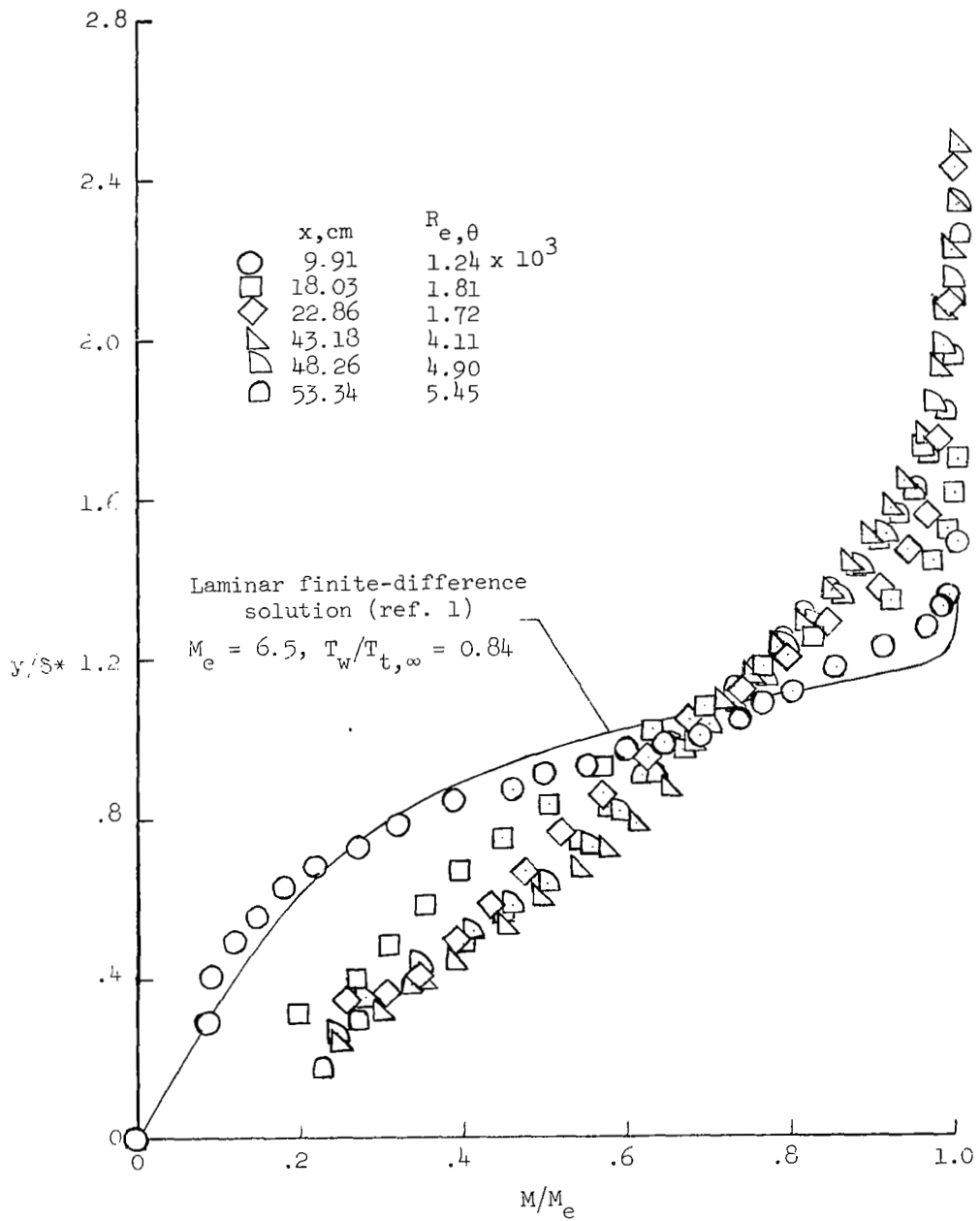
(b) Density profiles.

Figure 6.- Continued.



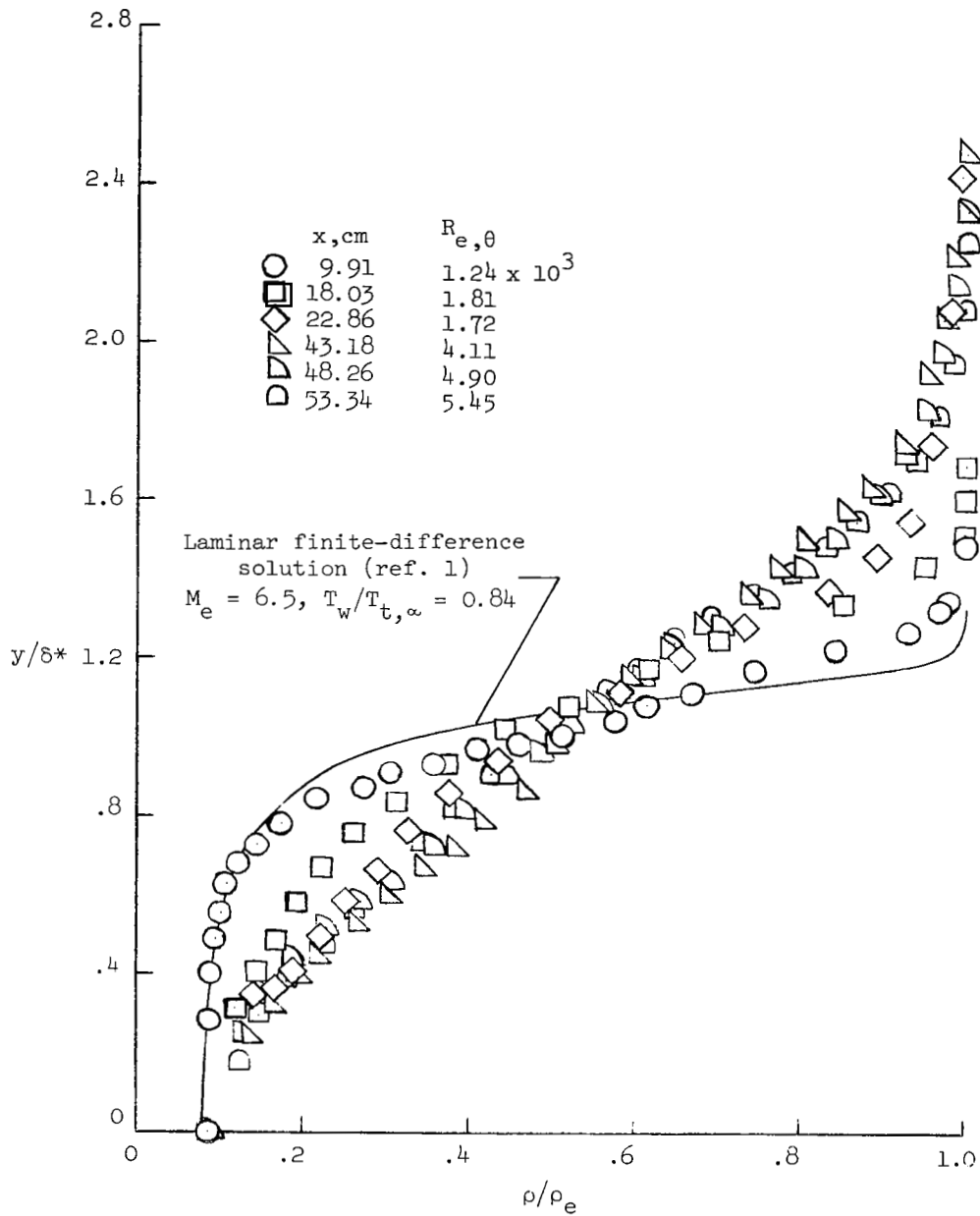
(c) Velocity profiles.

Figure 6. - Concluded.



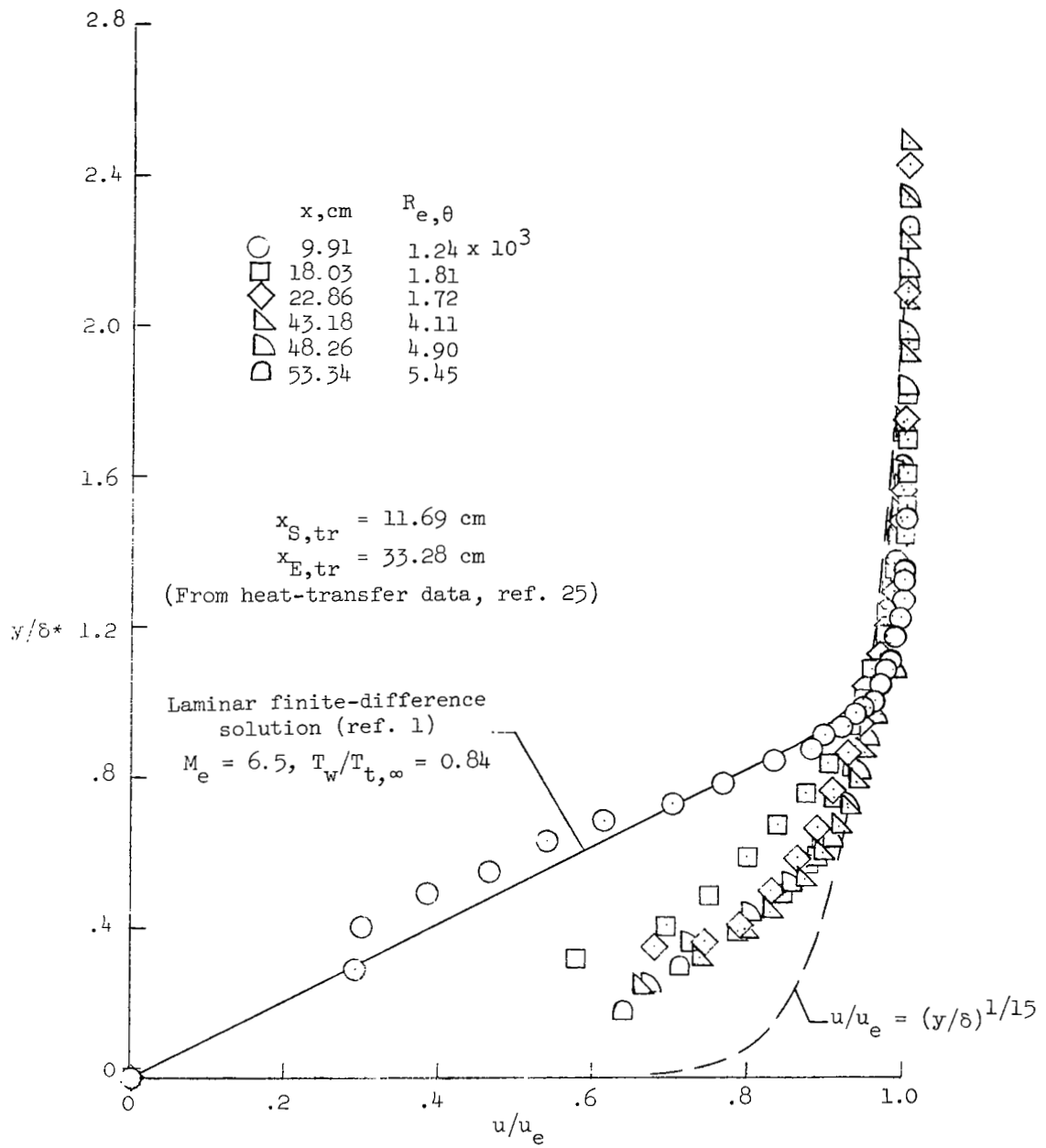
(a) Mach number profiles.

Figure 7.- Measured boundary-layer profiles at  $Re/cm = 0.255 \times 10^6$ .



(b) Density profiles.

Figure 7. - Continued.



(c) Velocity profiles.

Figure 7.- Concluded.

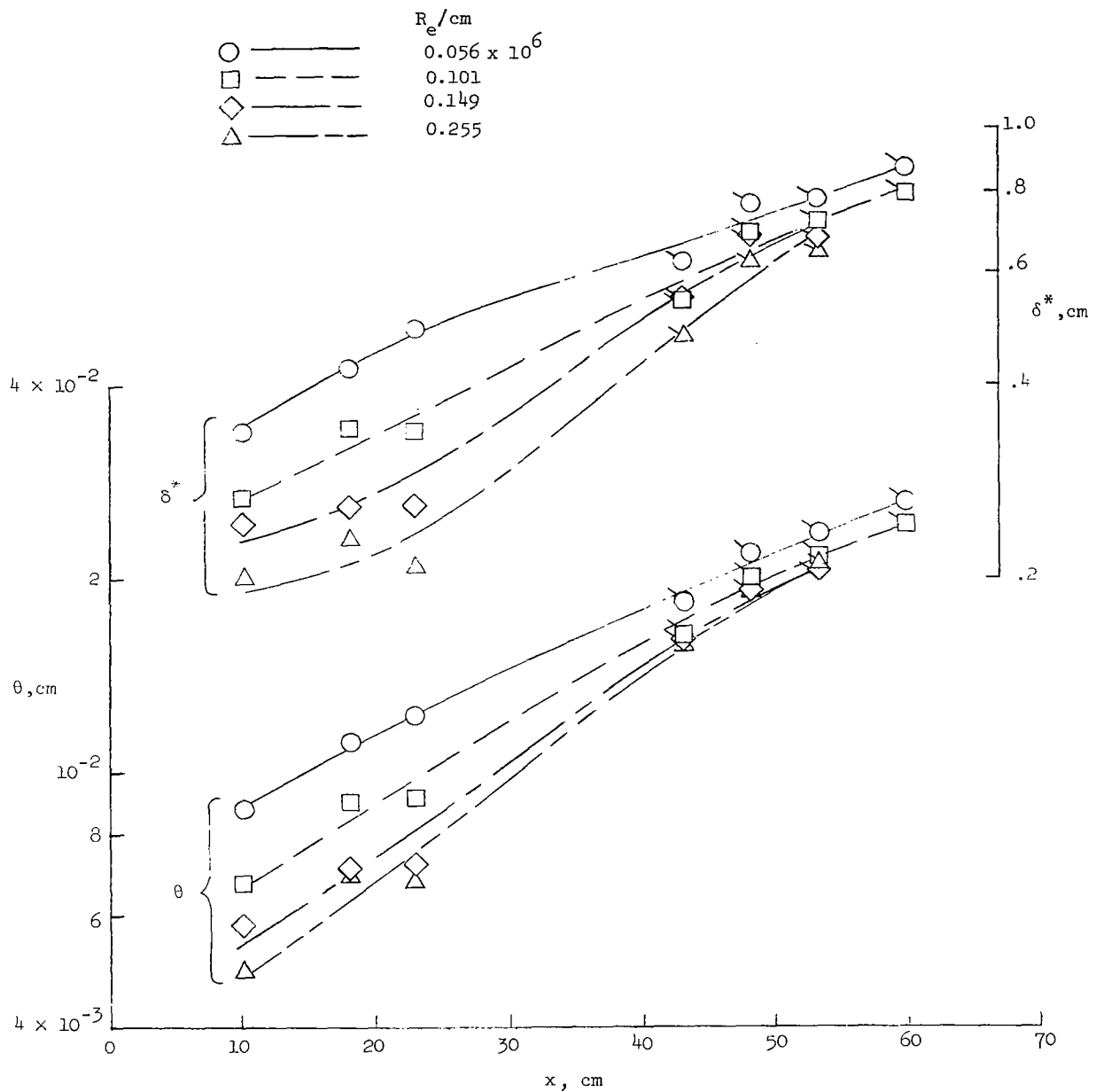


Figure 8.- Variation of displacement and momentum thickness along wedge. Flagged symbols represent data obtained on 60.96-cm wedge configuration.

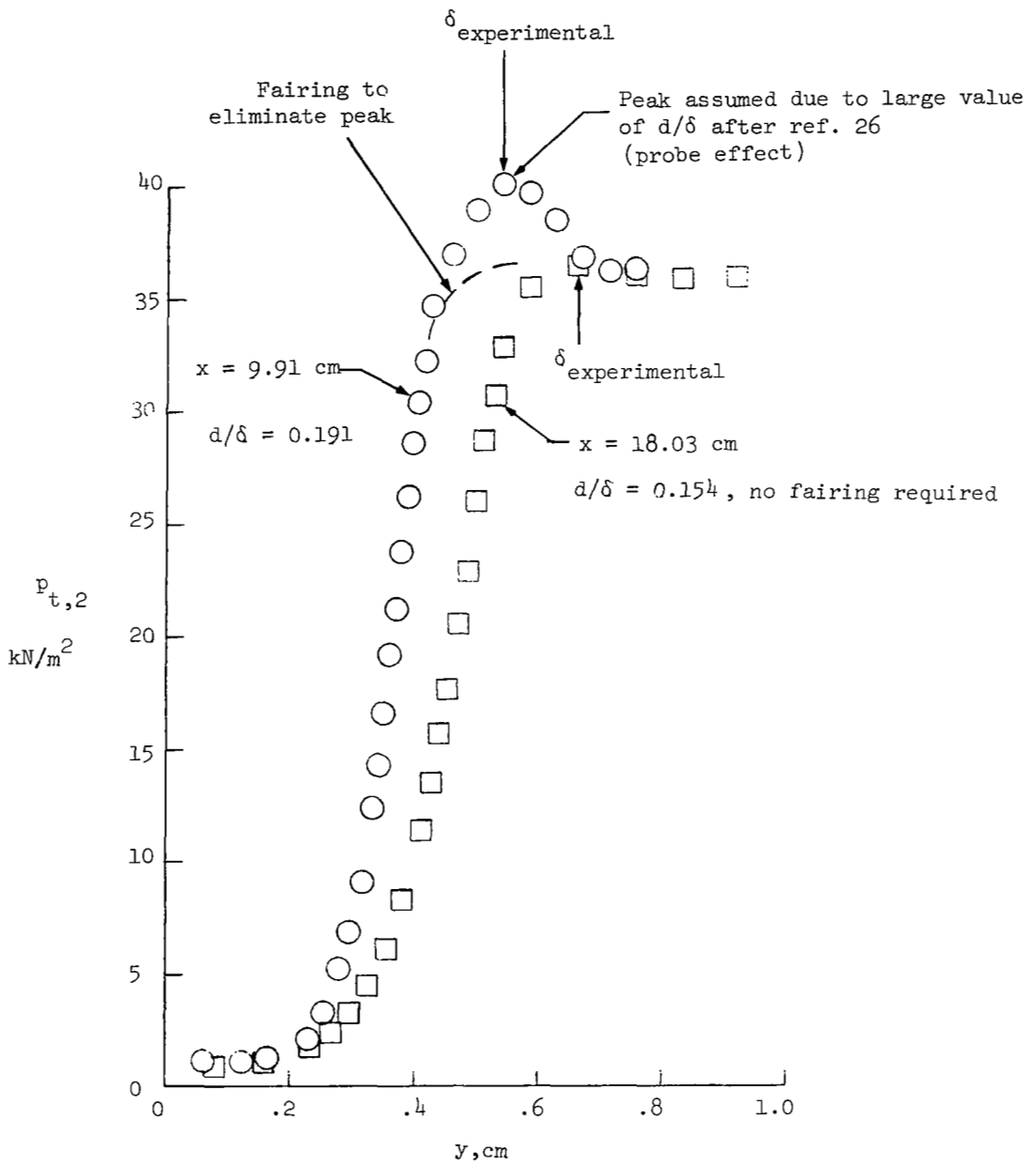
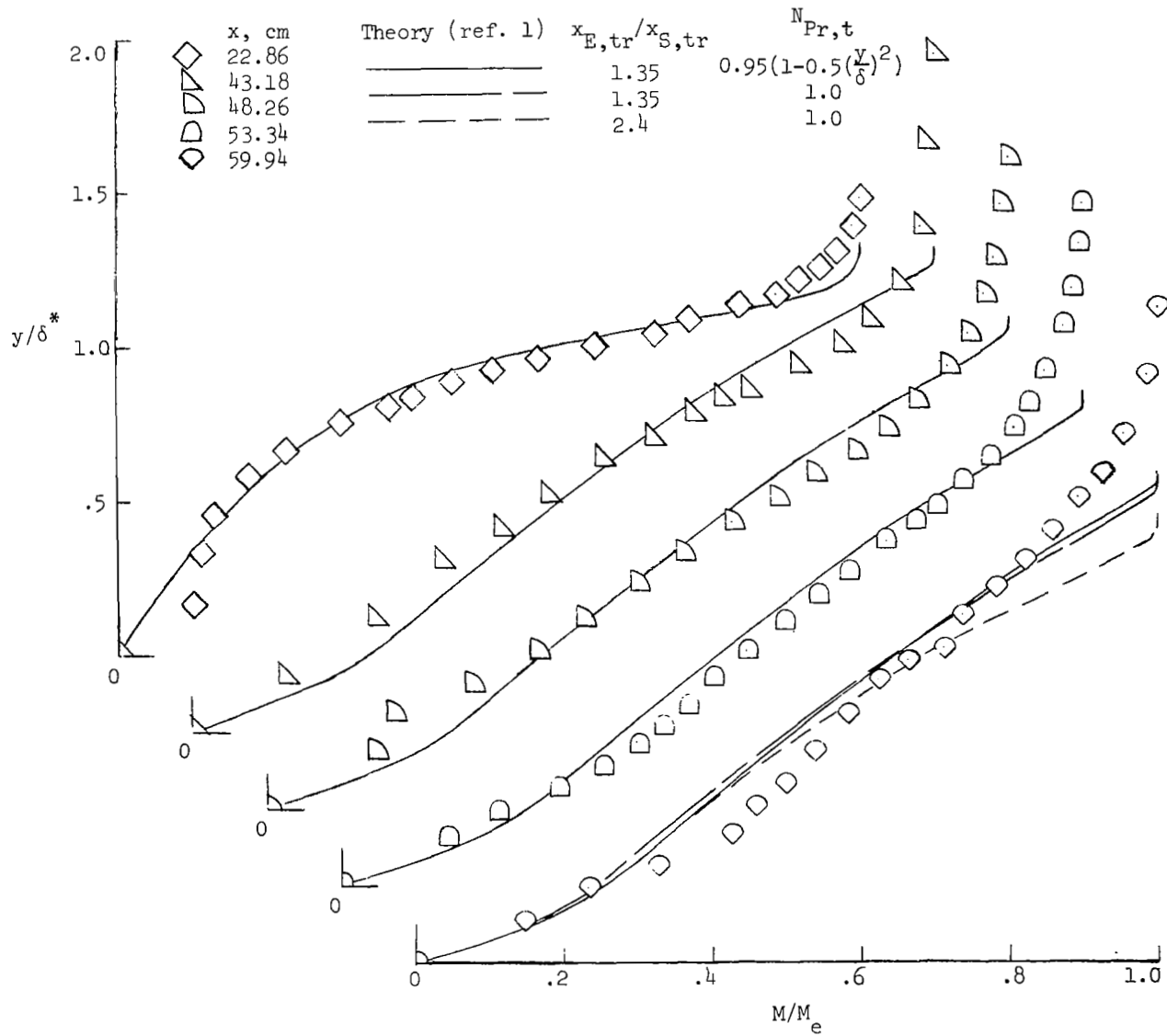
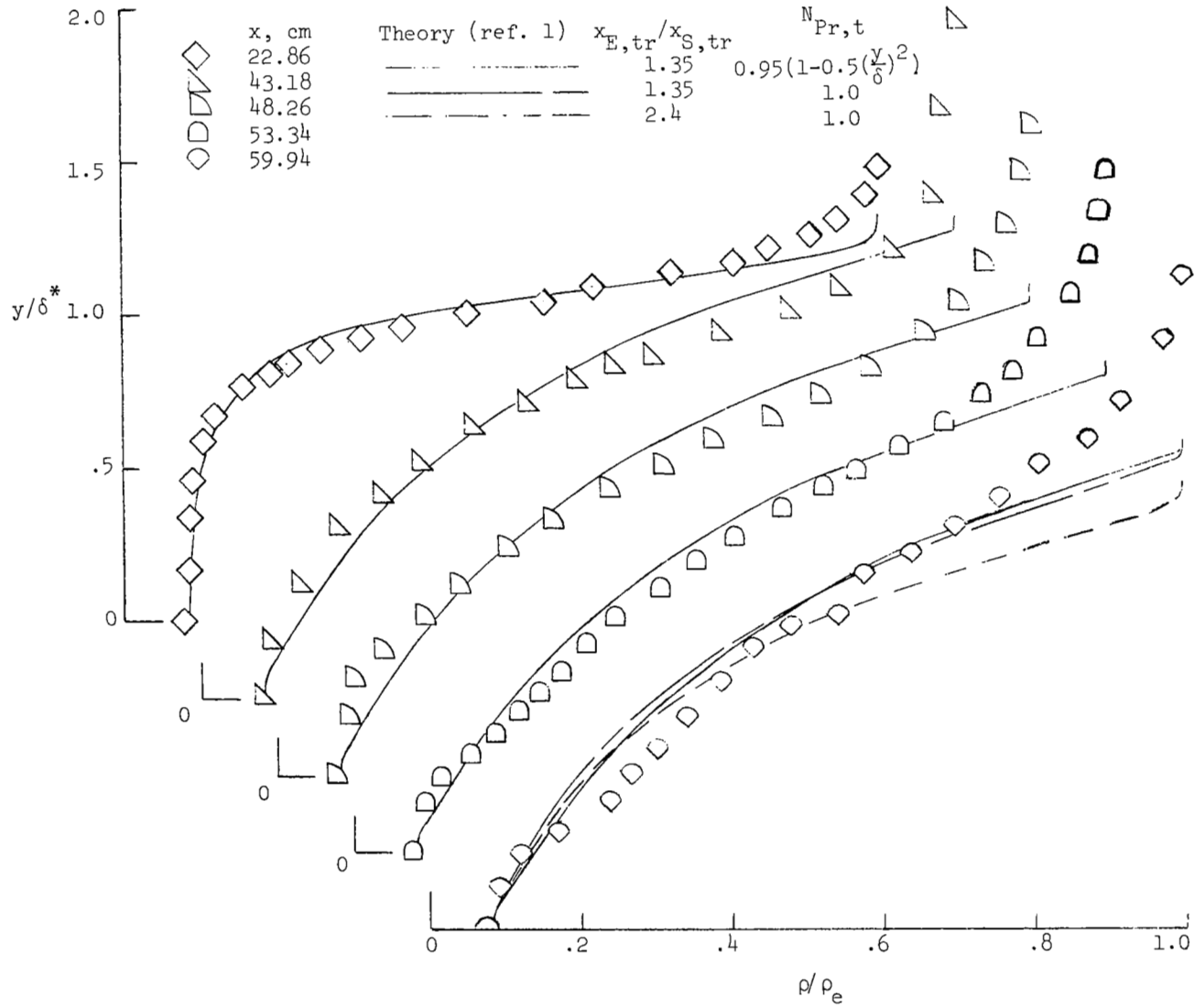


Figure 9. - Typical fairing of pitot data at boundary-layer edge when  $d/\delta \geq 0.19$ .  
 $Re/\text{cm} = 0.056 \times 10^6$ .



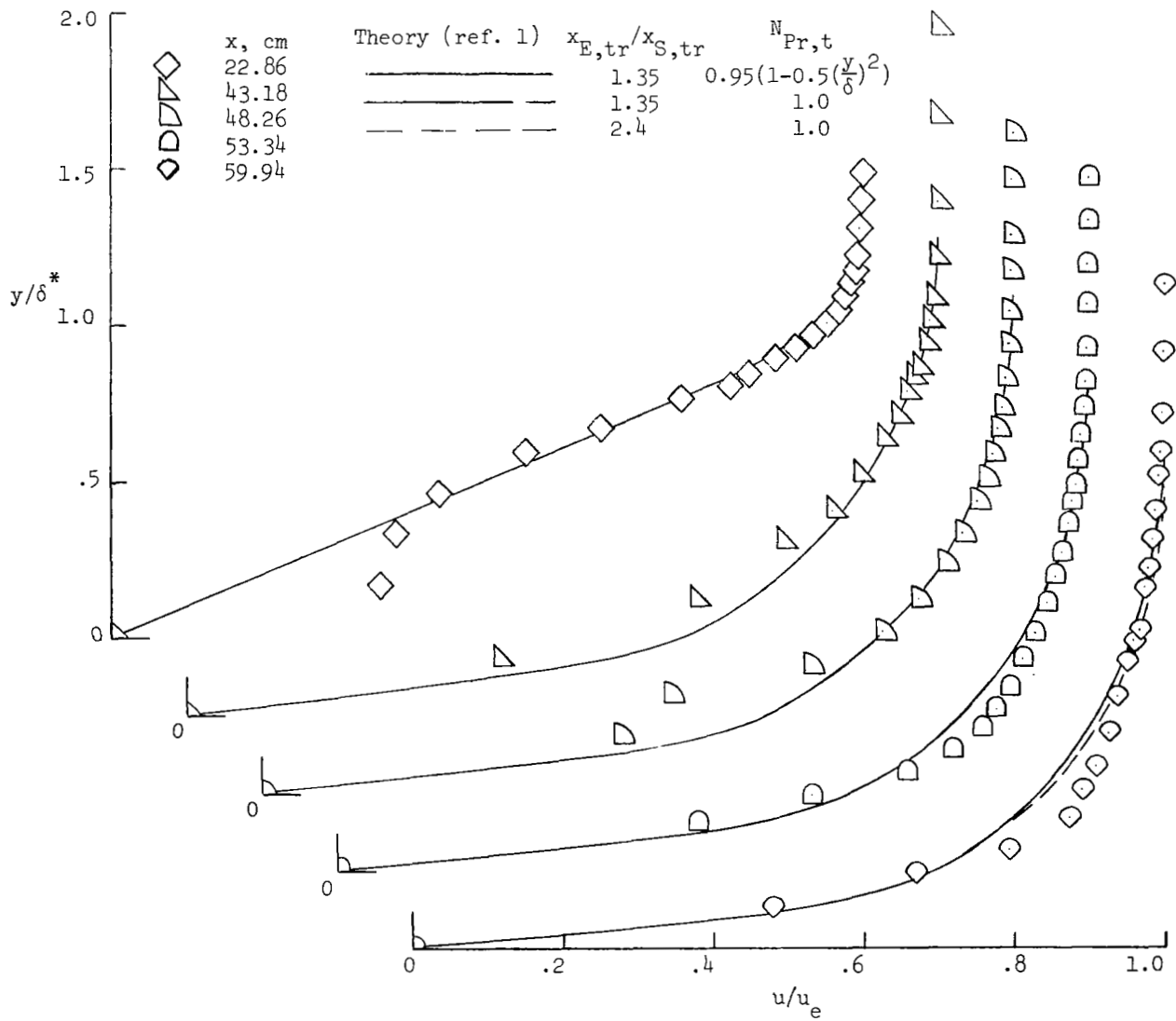
(a) Mach number profiles.

Figure 10.- Comparison of predicted and experimental profiles at  $Re/cm = 0.056 \times 10^6$ .



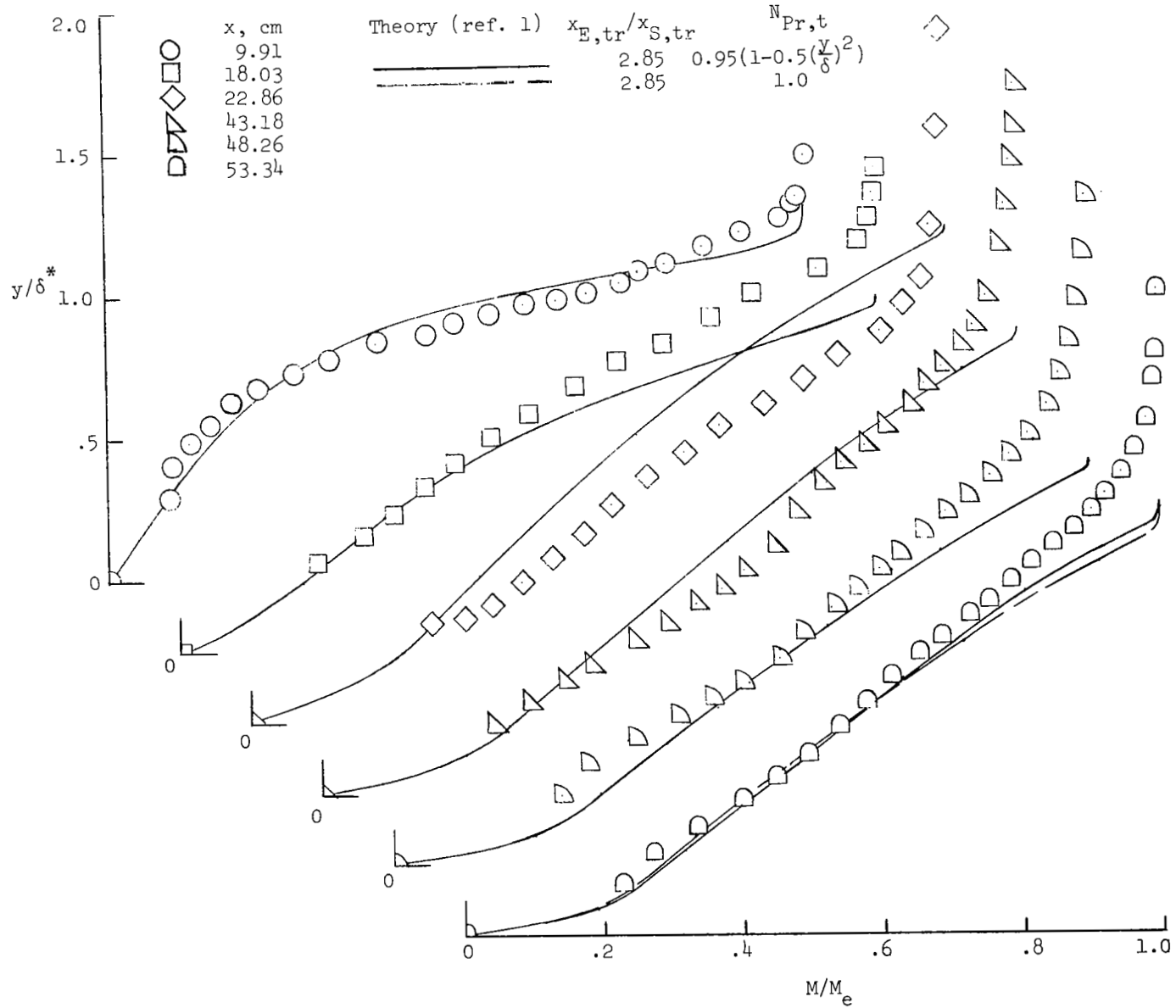
(b) Density profiles.

Figure 10.- Continued.



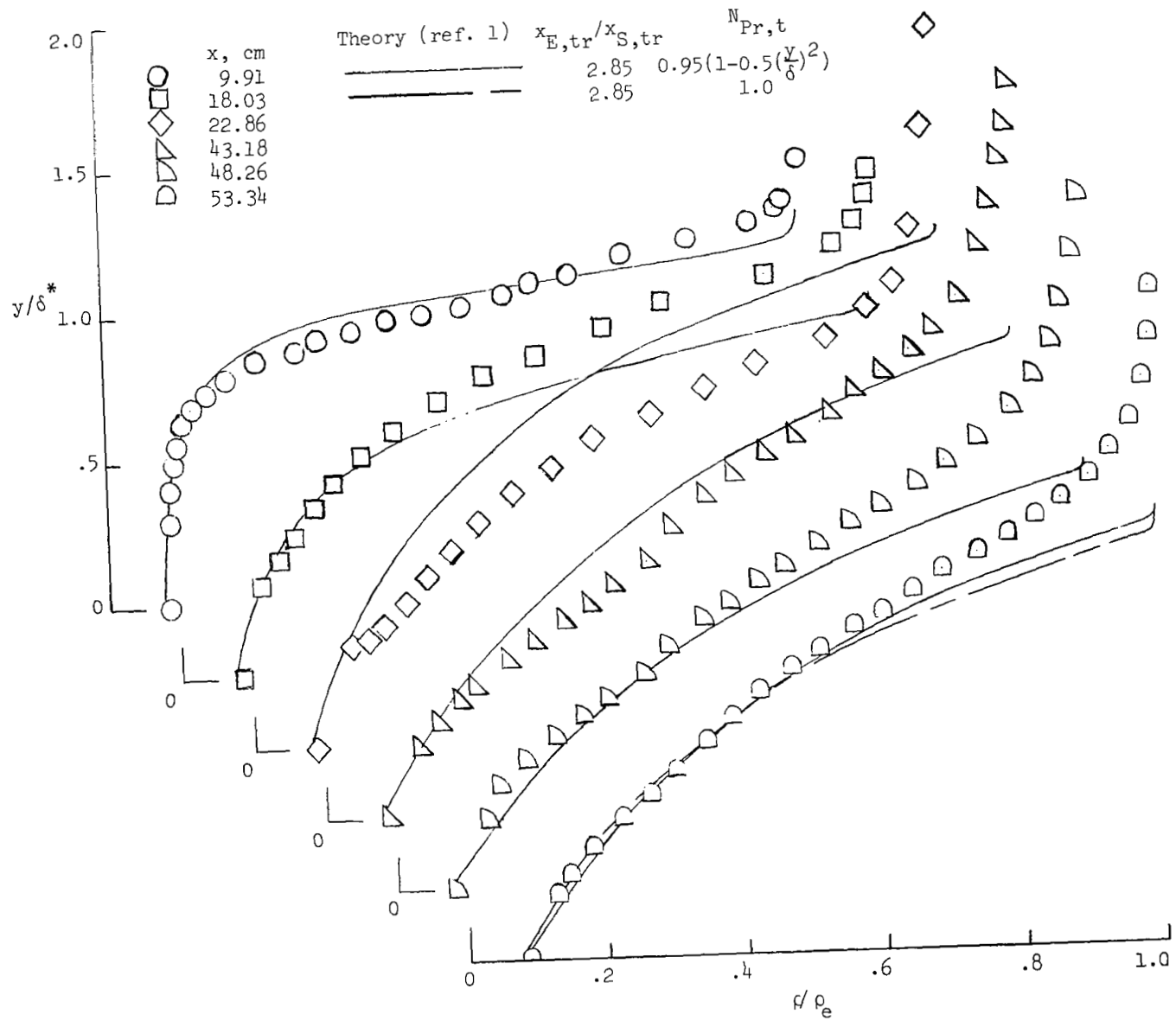
(c) Velocity profiles.

Figure 10.- Concluded.



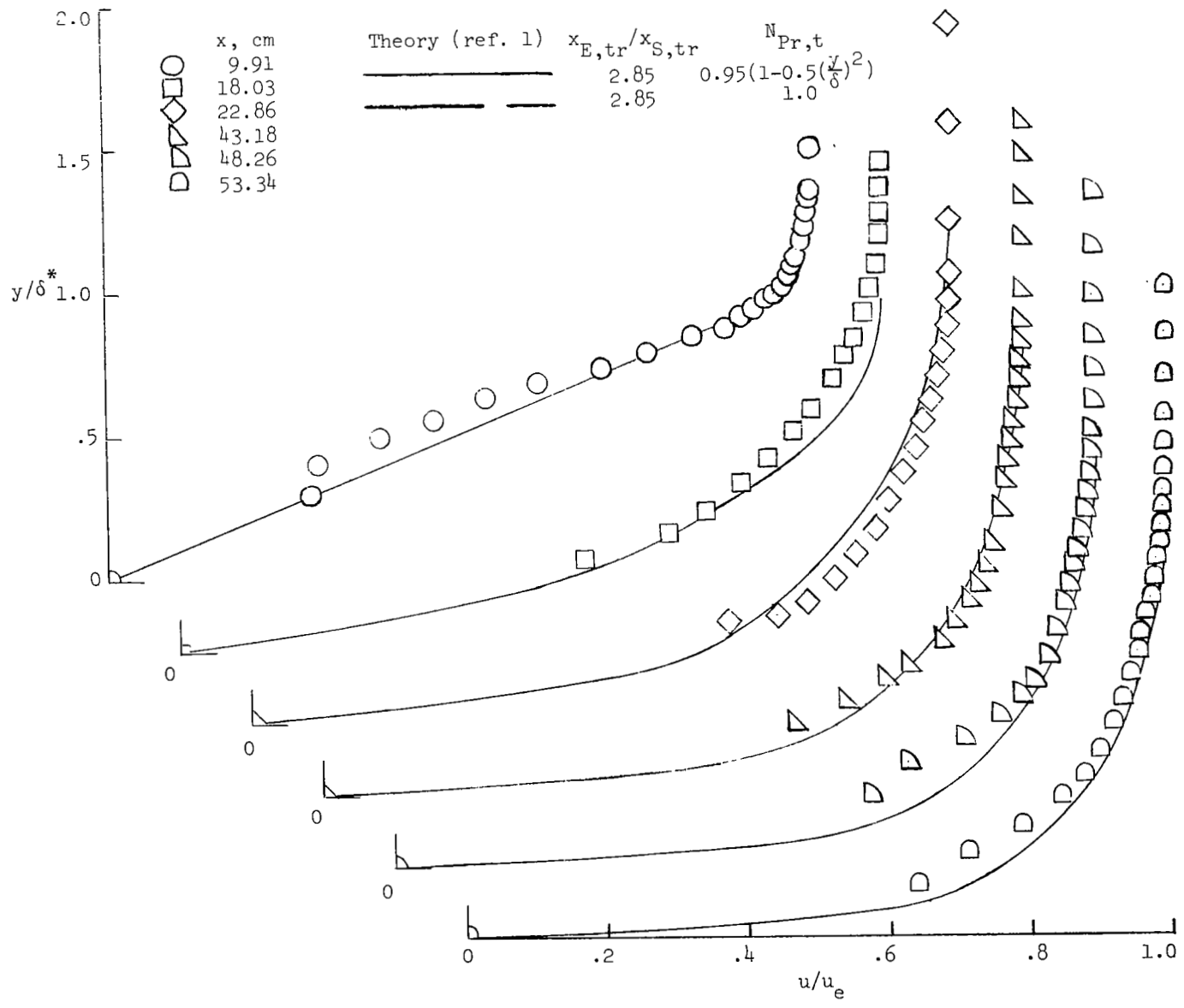
(a) Mach number profiles.

Figure 11.- Comparison of predicted and experimental profiles at  $Re/cm = 0.255 \times 10^6$ .



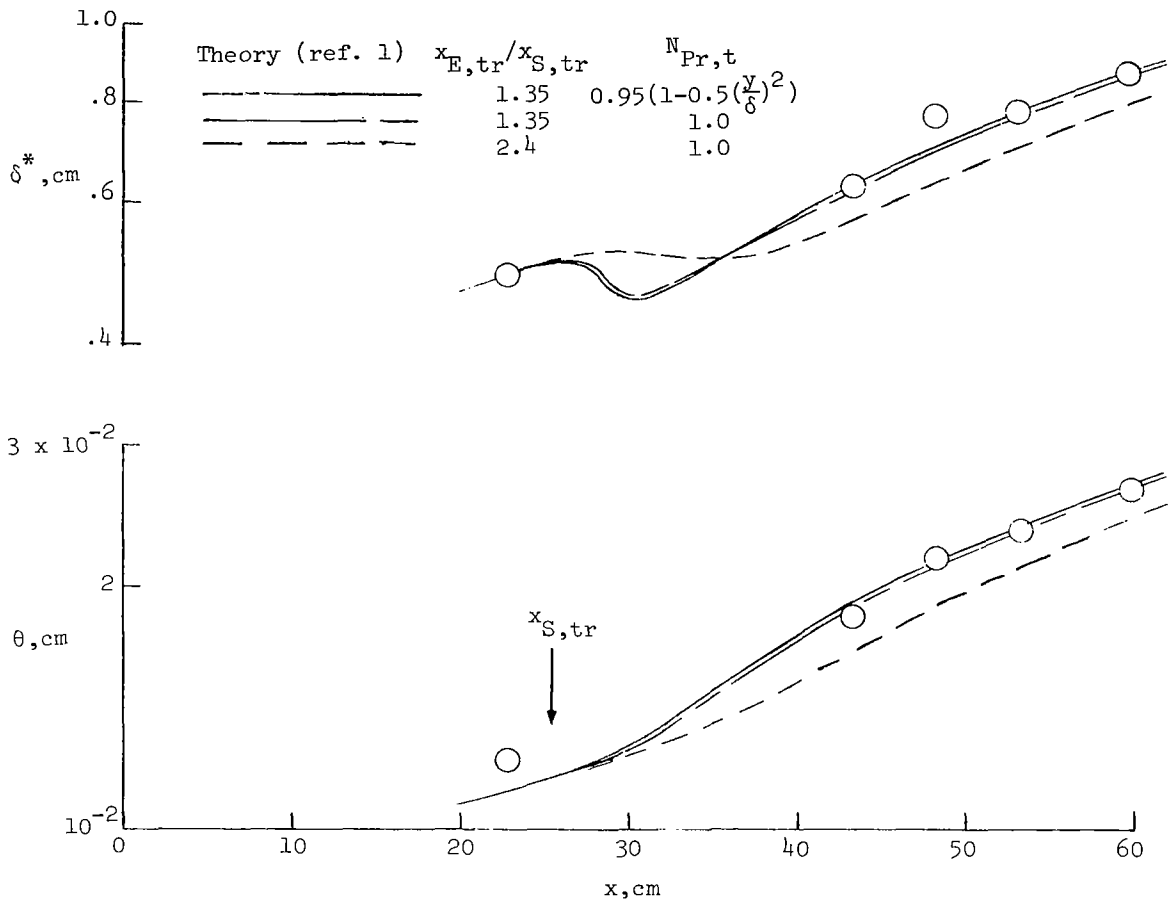
(b) Density profiles.

Figure 11.- Continued.



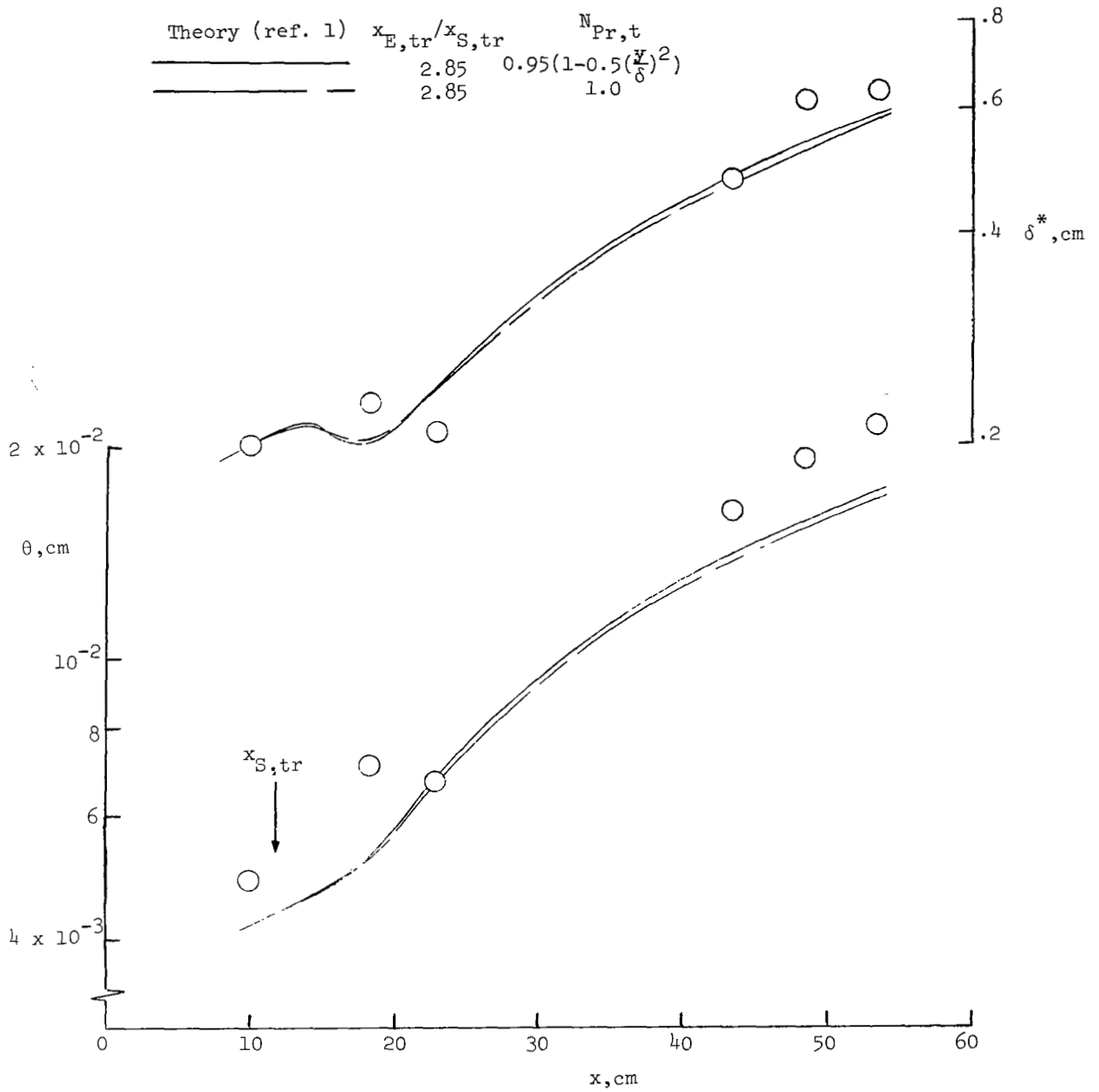
(c) Velocity profiles.

Figure 11.- Concluded.



(a)  $Re/cm = 0.056 \times 10^6$ .

Figure 12. - Comparison of predicted and experimental integral parameters along the wedge surface.



(b)  $Re/cm = 0.255 \times 10^6$ .

Figure 12.- Concluded.



014 001 C1 U 12 710902 S00903DS  
DEPT OF THE AIR FORCE  
AF SYSTEMS COMMAND  
AF WEAPONS LAB (WL0L)  
ATTN: E LOU BOWMAN, CHIEF TECH LIBRARY  
KIRTLAND AFB NM 87117

POSTMASTER: If Undeliverable (Section 158  
Postal Manual) Do Not Return

*"The aeronautical and space activities of the United States shall be conducted so as to contribute . . . to the expansion of human knowledge of phenomena in the atmosphere and space. The Administration shall provide for the widest practicable and appropriate dissemination of information concerning its activities and the results thereof."*

— NATIONAL AERONAUTICS AND SPACE ACT OF 1958

## NASA SCIENTIFIC AND TECHNICAL PUBLICATIONS

**TECHNICAL REPORTS:** Scientific and technical information considered important, complete, and a lasting contribution to existing knowledge.

**TECHNICAL NOTES:** Information less broad in scope but nevertheless of importance as a contribution to existing knowledge.

**TECHNICAL MEMORANDUMS:** Information receiving limited distribution because of preliminary data, security classification, or other reasons.

**CONTRACTOR REPORTS:** Scientific and technical information generated under a NASA contract or grant and considered an important contribution to existing knowledge.

**TECHNICAL TRANSLATIONS:** Information published in a foreign language considered to merit NASA distribution in English.

**SPECIAL PUBLICATIONS:** Information derived from or of value to NASA activities. Publications include conference proceedings, monographs, data compilations, handbooks, sourcebooks, and special bibliographies.

**TECHNOLOGY UTILIZATION PUBLICATIONS:** Information on technology used by NASA that may be of particular interest in commercial and other non-aerospace applications. Publications include Tech Briefs, Technology Utilization Reports and Technology Surveys.

*Details on the availability of these publications may be obtained from:*

**SCIENTIFIC AND TECHNICAL INFORMATION OFFICE**

**NATIONAL AERONAUTICS AND SPACE ADMINISTRATION**

**Washington, D.C. 20546**

